Heliyon 9 (2023) e18726

Contents lists available at ScienceDirect

Heliyon

journal homepage: www.cell.com/heliyon

Research article

Mathematical modeling and analysis of COVID-19 and TB co-dynamics

Zenebe Shiferaw Kifle *, Legesse Lemecha Obsu

Department of Mathematics, Adama Science and Technology University, Adama, Ethiopia

ARTICLE INFO

Keywords:
COVID-19
Tuberculosis
Mathematical model
Co-infection
Stability
Bifurcation analysis

ABSTRACT

This study proposes a mathematical model for examining the COVID-19 and tuberculosis (TB) co-dynamics thoroughly. First, the single infection dynamics: COVID-19 infection and TB infection models are taken into consideration and examined. Following that, the co-dynamics with TB and COVID-19 is also investigated. In order to comprehend the developed model dynamics, the basic system attributes including the region of definition, theory of nonnegativity and boundedness of solution are investigated. Further, a qualitative analysis of the equilibria of the formulated model equations is performed. The equilibria of both infection models are globally asymptotically stable if their respective basic reproductive number is smaller than one. As the associated reproductive number reaches unity, they experience the forward bifurcation phenomenon. Additionally, it is demonstrated that the formulated co-dynamics model would not experience backward bifurcation by applying the center manifold theory. Moreover, model fitting is done by using daily reported COVID-19 cumulative data in Ethiopia between March 13, 2020, and May 31, 2022. For instance, the non-linear least squares approach of fitting a function to data was performed in the fitting process using $scipy.optimize.curve\_fit$ from the Python. Finally, to corroborate the analytical findings of the model equation, numerical simulations were conducted.

1. Introduction

A new coronavirus family termed SARS-CoV-2 that was initially found in China is the cause of a communicable disease called Coronavirus Disease 2019 (COVID-19) [1]. Since then, it has rapidly spread across the world, raising major global concerns. This disease often causes mild to severe respiratory illness in its victims. Older people and people having medical issues including cancer, tuberculosis (TB), chronic respiratory conditions, diabetes, and cardiovascular disease are more prone to get seriously sick [2,3]. The signs of COVID-19 might vary based on the type of variant acquired, ranging from mild symptoms to a potentially fatal disease. Its clinical symptoms include fever, fatigue, dry cough, headache, sore throat, diarrhoea, and loss of scent or taste, whereas the symptoms in serious cases are chest discomfort or pressure, shortness of breath, loss of speech, or inability to move [4].

On the other hand, TB is an ancient but persistent present common and fatal pathogenic bacterial illness caused by *Mycobacterium tuberculosis* (MTB). It can transmit through sneeze, cough, speak, kiss or spit from people with active pulmonary TB. Transmission can only occur from active TB-infected people but not latent TB. TB is curable and preventable [5]. It remains very critical due to the fact if people do not take their drugs efficiently or they do not take the correct drugs they'll now no longer be cured. This is why

* Corresponding author.
E-mail addresses: zenebeshif16@gmail.com (Z.S. Kifle), legesse.lemecha@astu.edu.et (L.L. Obsu).

https://doi.org/10.1016/j.heliyon.2023.e18726
Received 8 September 2022; Received in revised form 17 July 2023; Accepted 25 July 2023

Available online 31 July 2023

such a lot of people nonetheless die from TB due to the fact their TB is not always absolutely cured. Worldwide, TB is still the biggest cause of mortality. Approximately 1.5 million people deceased from TB in 2020, and around 10 million contracted TB worldwide according to WHO TB report of 2021 [5]. Recently, some studies have shown that individuals infected with latent and active TB have a high risk of COVID-19 infection [6].

Co-epidemics necessitate a critical comprehension of the relationships between the diseases, their prevalence, and their mitigation in order to successfully manage these diseases. In the recent time, this has happened with TB and COVID-19. Currently, the co-infection of COVID-19 with comorbidities has been identified as the risk factors for increased COVID-19 cases and higher fatalities [7,8]. Both TB and COVID-19 are contagious diseases that predominantly affect the lungs, and they become serious public wellness problems and leave a dangerous mark on the next generation, particularly in sub-Saharan African countries and Asia. Patients who have both COVID-19 and TB may face poorer treatment outcomes, particularly if the TB medication is halted, because there is little prior experience with COVID-19 infection in TB sufferers. Cough, fever, and difficulty in breathing are common symptoms of both diseases. TB, however, has a prolonged incubation period with a later start of symptoms [9].

To achieve the relationships among COVID-19 and TB, many studies have been done [6,10–13]. For example, Chen et al. [6], found that TB might make people more susceptible to COVID-19 and make its symptoms more severe. According to the study given Petrone et al. [10], individuals who have TB and COVID-19 infection have a poor immunological response toward SARS-COV-2. In [11], it is demonstrated that the co-infection of individuals with both diseases are linked to increased mortality and deaths. Besides, as reported in [12], individuals who have ever experienced a TB infection are at a significant risk of dying if they get COVID-19. Additionally, as stated in [6], infected individuals with TB would be more likely to get COVID-19 regardless of how bad the condition is.

Infectious illness mathematical modeling has a long history and is increasingly utilized to comprehend transmission patterns, comprehend natural history more completely, organize research and public health treatments, assess treatments, and prepare for and react to outbreaks and epidemics. Since the COVID-19 outbreak, numerous mathematical models investigations have been conducted to look into the transmission dynamics by considering different scenarios [14–18] and the references cited therein. For instance, in [17], the authors formulated the COVID-19 model for evaluating and controlling its outbreak and used COVID-19 real data in Saudi Arabia for model validation. They verified the value of the presented model in analyzing the epidemic spread of COVID-19. Furthermore, various mathematical models for the COVID-19 co-infection with different illnesses have been proposed [19–21]. For example, Tchoumi et al. [21] proposed the first mathematical model which describes COVID-19 and malaria co-dynamics. They expanded the model to an optimal control and suggested that applying the protective measures for both diseases have a key role in reducing the spread compared to single prevention control measure.

Although some studies on COVID-19 and other illnesses co-infection have been conducted, recently, there is a limited number of studies for the dynamics of TB and COVID-19 co-infection models [22–25]. In particular, Omame et al. [22] proposed and examined a mathematical model of TB and COVID-19 co-dynamics using fractional order derivatives. They observed that minimizing the probability of contracting COVID-19 due to latent TB infection will reduce the burden of the COVID-19, and also their co-infection from the population. On the other hand, a mechanistic mathematical model of TB and COVID-19 co-dynamics is constructed and examined in [23]. They investigated that the effects of applying optimal control measures for COVID-19 and TB co-infection dynamics. In [24], another model is also addressed and it is shown that increasing the contact rate worsen the coinfection, while reducing the contacts and increasing the treatments could mitigate their spread. In [25] the co-dynamics model which contain the vaccination class is proposed and analyzed. According to their findings, either TB or SARS-CoV-2 mitigation mechanisms significantly reduced the number of new co-infections. More recently, a coinfection model to study the effect of isolation and treatment on reducing COVID-19 infection is proposed in [26]. They found that while medication has an effect that often takes longer to manifest, isolation had a direct effect in lowering the incidence of COVID-19 infections.

The co-infections of TB and COVID-19, however, require additional attention because both diseases are continually spreading and taking more lives. Thus, our aim is to explore the co-dynamics of TB and COVID-19 to better understand their spread and control through mathematical modeling and its analysis by employing a system of related models with various aspects. A further objective is to look into and discover their co-interactions in order to minimize their spread and effects substantially to recommend the policymakers. For that, a novel mathematical model which integrates the epidemiological traits of TB and COVID-19 is constructed. For instance, our model differs from the previous models as we considered some conceivable transmission pathways and recovering from either or both diseases. Further, the influence of COVID-19 personal protection strategy on the disease load is also considered. Our model complements earlier co-infection models, and is validated by a model fit to daily reported COVID-19 data in Ethiopia by using a non-linear least squares method, $scipy.optimize.curve\_fit$ function, from PYTHON.

The rest of the paper's content is organized in the manner described below. Section 2 presents the details of model formulation. In Section 3, the sub-models of COVID-19 and TB alone are provided and analytically investigated. Further, the stability analysis of the co-infection model also performed in Section 3.3. To support the theoretical findings, the numerical simulations of the co-dynamics model are discussed in Section 4. Lastly, the paper's conclusion is drawn in Section 5.

2. Model formulation

In this part, we develop the model with the intention of observing the transmission dynamics of COVID-19 and TB co-infection. To formulate our mathematical model, we take into considerations the following assumptions:

i) Susceptible populations are those who are under the risk of acquiring COVID-19 and TB infections at a rate proportional to the density of COVID-19 and TB infected people, respectively,
ii) No vertical transmission exists, all influxes (recruits) are born healthy and without infectious immigrants, and all parameters are positive,
iii) Co-infected individuals can transmit both diseases. Further, a person is more likely to transmit if a contact has already happened because of the impaired immune system. A contact in this context is any process that can transmit a disease.
iv) Co-infected individuals can not transmit mixed infections at the same time, they transmit only single infection [23],
v) TB infected individuals have an increased risk of susceptibility to COVID-19 [6],
vi) Individuals co-infected with both diseases are associated with higher mortality [11].

The entire number of people at time t, indicated by $N(t)$, is divided into eight divisions to construct the model: susceptible $S(t)$ who have not yet contracted either disease, infected individuals with latent TB $L(t)$, infectious TB class $I_t(t)$, infectious COVID-19 class $I_c(t)$, COVID-19 and latent TB co-infection class $I_{cL}(t)$, COVID-19-TB infectious class $I_{tc}(t)$, TB recovered class $R_t(t)$, and COVID-19 recovered class $R_c(t)$. Hence, the total human population is provided as

$$N(t) = S(t) + L(t) + I_c(t) + I_t(t) + I_{cL}(t) + I_{tc}(t) + R_c(t) + R_t(t).$$

Susceptible individuals acquire TB after becoming in contact with individuals in the classes I_t, and I_{tc}. Hence, the force of infection related to TB is provided by

$$\lambda_t = \frac{\beta_t(I_t + I_{tc})}{N}.$$

Further, susceptible individuals contract COVID-19 after becoming in contact with individuals in the classes I_c, I_{cL}, and I_{tc}. Hence, the force of infection related with COVID-19 becomes

$$\lambda_c = (1 - \kappa\rho)\frac{\beta_c(I_c + \tau(I_{tc} + I_{cL}))}{N}.$$

The parameters β_c and β_t represents the transmission coefficient of COVID-19 and TB, respectively. Here, we considered the standard incidence type of the forces of infection [27]. The parameter $\tau \geq 1$ represents the infectivity of individuals become co-infected due to TB, and $(1 - \rho\kappa)$ denotes effects of COVID-19 protection like physical distancing, sanitizer, washing hand, face mask, and self-isolation, where ρ (between 0 and 1) denotes efficacy of COVID-19 protection measure, and κ (between 0 and 1) is fraction of community applying COVID-19 protection measure.

Individuals infected with COVID-19 may contract TB at the rate $\omega\lambda_t$ and they become I_{cL}. The parameter $\omega \geq 1$ denotes the enhancement factor accounts for how infectiously susceptible people are to becoming TB after contracting COVID-19 disease. Individuals after being infected with TB join the latent TB infective class L or I_{cL}, and then move on to the class of people with active TB (I_t or I_{tc}) at a progression rate ϕ_t and η_c, respectively. At the rate $\nu\lambda_c$, TB recovered individuals acquire COVID-19 and become TB infected at the rate $\varphi\lambda_t$. These types' of transitions are widely used in many TB models and their co-dynamics [25,28–30], where ν and φ are the infectivity factor of TB recovered individuals to COVID-19 and TB respectively. Furthermore, we assume that COVID-19 recovered individuals become TB infected at the rate λ_t. Individuals having active TB may contract COVID-19 disease at the rate $\sigma\lambda_c$ and join I_{tc} class. The parameter $\sigma \geq 1$ denotes the modification parameter that shows the enhancement factor for individuals becoming COVID-19 infected as a result of TB. The descriptions of all transfers in the proposed model are shown in the schematic diagram given in Fig. 1. Further, the descriptions of the parameters in the model are summarized in Table 1. Following Fig. 1, we proposed the preceding governing system of ordinary differential equations

$$\begin{cases} \dot{S} = \Lambda - (\lambda_c + \lambda_t + \mu)S, \\ \dot{L} = \lambda_t S + \eta_L I_{cL} + \varphi\lambda_t R_t + \lambda_t R_c - (\lambda_c + \phi_t + r_L + \mu)L, \\ \dot{I}_c = \lambda_c S + \alpha_c I_{tc} + \nu\lambda_c R_t - (\omega\lambda_t + r_c + \delta_1 + \mu)I_c, \\ \dot{I}_t = \phi_t L + \theta I_{tc} - (\sigma\lambda_c + r_t + \delta_2 + \mu)I_t, \\ \dot{I}_{cL} = \lambda_c L + \omega\lambda_t I_c - (\eta_c + \eta_L + \mu)I_{cL}, \\ \dot{I}_{tc} = \sigma\lambda_c I_t + \eta_c I_{cL} - (\alpha_c + \theta + \delta_3 + \mu)I_{tc}, \\ \dot{R}_c = r_c I_c - (\lambda_t + \mu)R_c, \\ \dot{R}_t = r_L L + r_t I_t - (\varphi\lambda_t + \nu\lambda_c + \mu)R_t, \end{cases} \tag{1}$$

with initial conditions

$$\begin{cases} S(0) > 0,\ L(0) \geq 0,\ I_c(0) \geq 0,\ I_t(0) \geq 0, \\ I_{cL}(0) \geq 0,\ I_{tc}(0) \geq 0,\ R_t(0) \geq 0,\ R_c(0) \geq 0. \end{cases} \tag{2}$$

3. Model analysis

In order to carryout the qualitative analysis of the model, initially we analyze the single infection models as given below.

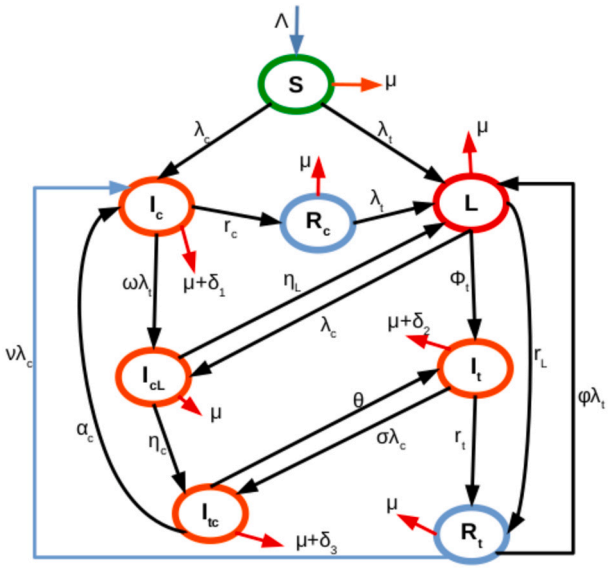

Fig. 1. A flow chart that shows the co-dynamics of COVID-19 and TB.

Table 1
Definitions of model parameters.

Parameters	Parameter descriptions
Λ	Influx rate
μ	Natural death rate
δ_1	COVID-19 induced death rate
δ_2	TB induced death rate
δ_3	COVID-19-TB co-infection induced death rate
β_c	COVID-19 transmission rate
β_t	TB transmission rate
r_c	COVID-19 recovery rate for individuals in I_c class
r_t	TB recovery rate for individuals in I_t class
r_L	Latent TB recovery rate
α_c	TB recovery rate for individuals in I_{tc} class
ϕ_t, η_c	Progression rate from latent classes to active TB
η_L, θ	Recovery rates from COVID-19 for the classes I_cL and I_tc, respectively

3.1. COVID-19 sub-model

By setting $I_t(t) = I_{cL}(t) = I_{tc}(t) = R_t(t) = 0$ in system (1), we get the COVID-19 sub-model:

$$\begin{cases} \dot{S} = \Lambda - (\lambda_c + \mu)S, \\ \dot{I}_c = \lambda_c S - (r_c + \delta_1 + \mu)I_c, \\ \dot{R}_c = r_c I_c - \mu R_c, \end{cases} \tag{3}$$

where $\lambda_c = (1 - \kappa\rho)\dfrac{\beta_c I_c}{N}$, $N = S(t) + I_c(t) + R_c(t)$.

3.1.1. Nonnegativity of the solution

Theorem 1. *Given the initial data* (2)*, the sub-model* (3) *remain non-negative for all* $t \geq 0$.

Proof. Having the first equation of the model (3), we get

$$\frac{dS}{dt} = \Lambda - (\lambda_c + \mu)S.$$

When the positive term Λ is omitted, the aforementioned equation reduces to

$$\frac{dS}{dt} \geq -(\lambda_c + \mu)S.$$

Using integration to solve for variable S results in

$$S(t) \geq S(0)e^{\int_0^t (\lambda_c(\xi)+\mu)d\xi} \geq 0,$$

which implies the nonnegativity of $S(t)$ for all time t.
Similarly, from the second and third equation of the model (3), we obtain

$$I_c(t) \geq I_c(0)e^{\int_0^t \left((1-\kappa\rho)\beta_c \frac{S(\xi)}{N} - (r_c+\delta_1+\mu)\right)d\xi} \geq 0.$$
$$R_c(t) \geq R_c(0)e^{-\mu t} \geq 0.$$

Therefore, the solution to model (3) is non-negative for every $t \geq 0$. □

3.1.2. Region of invariance

Theorem 2. *The region*

$$\Omega_C = \left\{ (S, I_c, R_c) \in \mathbb{R}^3_+ : N(t) \leq \frac{\Lambda}{\mu} \right\}$$

is positively invariant for the system (3).

Proof. By adding up the right-hand sides of the COVID-19 sub-model (3), we have

$$\dot{N} = \Lambda - \mu N - \delta_1 I_c. \tag{4}$$

From the initial values (2), we have that $N(0) \geq 0$. Further, it follows, from equation (4), that

$$\dot{N} \leq \Lambda - \mu N. \tag{5}$$

Solving equation (5), we arrived at

$$N(t) \leq N(0)e^{-\mu t} + \frac{\Lambda}{\mu}(1 - e^{-\mu t}).$$

For a large positive t, we have $0 \leq N(t) \leq \frac{\Lambda}{\mu}$. Thus, in the region

$$\Omega_C = \left\{ (S, I_c, R_c) \in \mathbb{R}^3_+ : N(t) \leq \frac{\Lambda}{\mu} \right\},$$

every solution of model (3) initiating in Ω_C stay there for all $t \geq 0$ [31,32]. That is, Ω_C is positively invariant and attracts [33]. Hence, it is sufficient to study the dynamics of the COVID-19 sub-model (3) in Ω_C [23,34,35]. □

3.1.3. Disease-free equilibrium and basic reproduction number

The disease free equilibrium (DFE) of the COVID-19 system (3) is calculated by equating it to zero and putting $I_c = 0$. Then, we get

$$E_c^0 = (S^0, I_c^0, R_c^0) = \left(\frac{\Lambda}{\mu}, 0, 0\right).$$

To obtain basic reproductive number R_{0_c} for system (3), we used the next generation matrix method [36,37] so that R_{0_c} is calculated from the Jacobian matrix FV^{-1} computed at E_c^0.
Considering the infected compartment I_c, system (3) rewritten as

$$\dot{x} = f(x) = \mathcal{F}(x) - \mathcal{V}(x),$$

where

$$\mathcal{F} = \left[(1-\kappa\rho)\beta_c \frac{S I_c}{N} \right] \quad \text{and} \quad \mathcal{V} = \left[(r_c + \delta_1 + \mu) I_c \right].$$

As a result, when we evaluate the corresponding Jacobian matrices at E_c^0, we get

$$F = \left[(1-\kappa\rho)\beta_c \right] \quad \text{and} \quad V = \left[r_c + \delta_1 + \mu \right].$$

Then, the next generation matrix is provided as,

$$FV^{-1} = \left[\frac{(1-\kappa\rho)\beta_c}{(r_c + \delta_1 + \mu)} \right],$$

and thus the basic reproduction number for system (3) is

$$R_{0_c} = \frac{(1-\kappa\rho)\beta_c}{(r_c+\delta_1+\mu)}. \tag{6}$$

Remark 1. The basic reproduction number can be defined as the expected number of secondary infectious cases generated by one infectious individual during his or her infectious period in a fully susceptible population [37].

3.1.4. Disease-free equilibrium and its stability analysis

Theorem 3. *The equilibrium, E_c^0, of system (3) is locally asymptotically stable (LAS) for $R_{0_c} < 1$ and unstable when $R_{0_c} > 1$.*

Proof. To prove the theorem, we compute system (3) at E_c^0, which is given by

$$J_{E_c^0} = \begin{pmatrix} -\mu & -(1-\kappa\rho)\beta_c & 0 \\ 0 & (1-\kappa\rho)\beta_c - (r_c+\delta_1+\mu) & 0 \\ 0 & r_c & -\mu \end{pmatrix},$$

and its eigenvalues are the roots of

$$(-\mu-\lambda)(-\mu-\lambda)([(1-\kappa\rho)\beta_c - (r_c+\delta_1+\mu)]-\lambda) = 0.$$

Thus, the eigenvalues are

$$\lambda_1 = -\mu = \lambda_2 \quad \text{and} \quad \lambda_3 = (1-\kappa\rho)\beta_c - (r_c+\delta_1+\mu).$$

The eigenvalues λ_1 and λ_2 have negative real parts. We can rewrite the eigenvalue λ_3 as

$$\lambda_3 = (1-\kappa\rho)\beta_c - (r_c+\delta_1+\mu) = (r_c+\delta_1+\mu)\left(\frac{(1-\kappa\rho)\beta_c}{(r_c+\delta_1+\mu)} - 1\right) = (r_c+\delta_1+\mu)(R_{0_c}-1),$$

which have negative real part if and only if $R_{0_c} < 1$. Thus, all the eigenvalues of the Jacobian matrix $J_{E_c^0}$ are negative for if $R_{0_c} < 1$. As a result, system (3) has a LAS DFE, E_c^0, when $R_{0_c} < 1$ and unstable if $R_{0_c} > 1$. □

Theorem 4. *The DFE of the TB sub-model (3) is globally asymptotically stable (GAS) whenever $R_{0_t} < 1$.*

Proof. Define the Lyapunov function as

$$V = I_c.$$

The time derivative of V becomes

$$\begin{aligned} \dot{V} &= \dot{I}_c \\ &= \lambda_c S - (r_c+\delta_1+\mu)I_c \\ &= [(1-\kappa\rho)\beta_c \frac{S}{N} - (r_c+\delta_1+\mu)]I_c \\ &\le [(1-\kappa\rho)\beta_c - (r_c+\delta_1+\mu)]I_c \\ &= (r_c+\delta_1+\mu)I_c\,(R_{0_c}-1) \\ &\le 0, \text{ for } R_{0_c} \le 1. \end{aligned}$$

It can be seen that $\dot{V} \le 0$ for $R_{0_c} \le 1$, with $\dot{V} = 0$ if and only if $I_c = 0$. Substituting $I_c = 0$ into (3) shows that $S \longrightarrow \frac{\Lambda}{\mu}$ as $t \longrightarrow \infty$. Thus, the largest compact invariant set in $\{(S, I_c, R_c) \in \Omega_C : \dot{V} = 0\}$ is E_c^0. Therefore, using LaSalle's invariance principle [38], every solution of (3), with initial conditions in Ω_C approaches E_c^0, as $t \longrightarrow \infty$ for $R_{0_c} \le 1$. □

3.1.5. Existence and stability of endemic equilibrium of system (3)

We now investigate the existence and stability of the endemic equilibrium (EE) for COVID-19 sub-model (3).

Theorem 5. *The COVID-19 sub-model has a unique EE if and only if $R_{0_c} > 1$.*

Proof. To determine the EE equilibrium of system (3), we have to calculate given below:

$$\begin{cases} \Lambda - (\mu + \lambda_c^*)S^* = 0, \\ \lambda_c^* S^* - (r_c + \delta_1 + \mu)I_c^* = 0, \\ r_c I_c^* - \mu R_c^* = 0, \end{cases} \tag{7}$$

where $\lambda_c^* = (1-\kappa\rho)\beta_c \dfrac{I_c^*}{N^*} = (1-\kappa\rho)\beta_c \dfrac{I_c^*}{S^* + I_c^* + R_c^*}$.

From system (7), solving for S^*, I_c^* and R_c^*, we get the EE of sub-model (3)

$$\begin{aligned} S^* &= \frac{\Lambda(r_c+\mu)R_{0_c}}{\mu[(1-\kappa\rho)\beta_c(R_{0_c}-1)+(r_c+\mu)R_{0_c}]}, \\ I_c^* &= \frac{\mu(R_{0_c}-1)}{\mu + r_c}S^*, \\ R_c^* &= \frac{r_c}{\mu}I_c^*. \end{aligned} \tag{8}$$

It is easily observed from (8) that the sub-model (3) has a unique EE when $R_{0_c} > 1$, but does not have any EE when $R_{0_c} < 1$. □

The next result arises from Theorem 2 provided in [37].

Theorem 6. ***(Local stability of EE:)*** *The unique EE, E_c^*, of system (3) is LAS if $R_{0_c} > 1$ otherwise unstable.*

3.1.6. Bifurcation analysis

This section presents the direction of the bifurcation, forward or backward, i.e., the exchange of stability for DFE with an EE based on threshold value R_{0_c}. A model with globally stable equilibrium means it does not show the phenomenon of backward bifurcation, which occurs when a stable DFE coexists with a stable EE [21,23,34,35]. We use the center manifold theory as described in Theorem 4.1 from [39]. It is first necessary to simplify and change variables in order to apply this theory.

Denote $x = (x_1, x_2, x_3)^T = (S, I_c, R_c)^T$. Then system (3) is rewritable as follows:

$$\begin{cases} \dfrac{dx_1}{dt} = f_1(x) = \Lambda - (1-\kappa\rho)\beta_c \dfrac{x_1 x_2}{x_1+x_2+x_3} - \mu x_1, \\ \dfrac{dx_2}{dt} = f_2(x) = (1-\kappa\rho)\beta_c \dfrac{x_1 x_2}{x_1+x_2+x_3} - (r_c+\delta_1+\mu)x_2, \\ \dfrac{dx_3}{dt} = f_3(x) = r_c x_2 - \mu x_3. \end{cases} \tag{9}$$

Considering the case $R_{0_c} = 1$, and selecting β_c^* as the bifurcation parameter, we get

$$\beta_c = \beta_c^* = \frac{(r_c+\delta_1+\mu)}{1-\kappa\rho}.$$

The linearization of system (9) at E_c^0 and $\beta_c = \beta_c^*$ is given by

$$J_{(E_c^0, \beta_c^*)} = \begin{pmatrix} -\mu & -(r_c+\delta_1+\mu) & 0 \\ 0 & 0 & 0 \\ 0 & r_c & -\mu \end{pmatrix}.$$

Clearly, the eigenvalues of $J_{(E_c^0,\beta_c^*)}$ are $-\mu$, 0, and $-\mu$. This implies E_c^0 is non-hyperbolic. Hence, we can apply the Castillo-Chavez and Song [39] to investigate the dynamics of the system (9) near $\beta_c = \beta_c^*$. Indeed, we carry on as follows.

Representing the right eigenvector of the system (9) by $w = (w_1, w_2, w_3)^T$ and solving for

$$J_{(E_c^0,\beta_c^*)} \cdot w = 0,$$

we get the right eigenvectors

$$w_1 = -\frac{(r_c+\delta_1+\mu)}{r_c}w_3, \quad w_2 = \frac{\mu}{r_c}w_3, \quad w_3 = w_3 > 0.$$

Likewise, representing the left eigenvector of the system (9) by $v = (v_1, v_2, v_3)$ and solving for

$$v \cdot J_{(E_c^0,\beta_c^*)} = 0,$$

we get the left eigenvectors

$$v_1 = 0, \quad v_3 = 0, \quad v_2 = v_2 > 0.$$

The two eigenvectors must fulfill the condition $v \cdot w = 1$, i.e.,

$$\frac{\mu}{r_c} v_2 w_3 = 1.$$

Direction of the bifurcation: The coefficients of the bifurcation at E_c^0 are given as

$$a = \sum_{k,i,j=1}^{3} v_k w_i w_j \frac{\partial^2 f_k}{\partial x_i \partial x_j}(E_c^0, \beta_c^*)$$
$$b = \sum_{k,i=1}^{3} v_k w_i \frac{\partial^2 f_k}{\partial x_i \partial \beta_c}(E_c^0, \beta_c^*).$$

Since $v_1 = 0$ and $v_3 = 0$, all that is required are the partial derivatives of f_2, where

$$f_2 = \frac{\beta_c x_1 x_2}{x_1 + x_2 + x_3} - (r_c + \delta_1 + \mu) x_2.$$

Computing the 2nd order partial derivatives of f_2 at (E_c^0, β_c^*), we have the followings nonzero derivatives:

$$\frac{\partial^2 f_2}{\partial x_3 \partial x_2}(E_c^0, \beta_c^*) = -(1 - \kappa\rho)\frac{\beta_c^* \mu}{\Lambda}, \quad \text{and} \quad \frac{\partial^2 f_2}{\partial x_2^2}(E_c^0, \beta_c^*) = -2(1 - \kappa\rho)\frac{\beta_c^* \mu}{\Lambda}.$$

Furthermore,

$$\frac{\partial^2 f_2}{\partial x_2 \partial \beta_c}(E_c^0, \beta_c^*) = (1 - \kappa\rho).$$

To ascertain the type of the bifurcation, we need to calculate and find out the sign for a and b, which are bifurcation coefficients evaluated at the DFE (E_c^0). Hence, we obtain

$$\begin{aligned} a &= v_2 \left[2 w_2 w_3 \frac{\partial^2 f_2}{\partial x_2 \partial x_3} + w_2^2 \frac{\partial^2 f_2}{\partial x_2^2} \right] \\ &= -2 v_2 \frac{\mu(r_c + \delta_1 + \mu)}{\Lambda} \left(w_3 w_2 + w_2^2 \right) < 0, \\ b &= v_2 \left(w_2 \frac{\partial^2 f_2}{\partial x_2 \partial \beta_c} \right) \\ &= (1 - \kappa\rho) v_2 w_2 > 0. \end{aligned}$$

Because $a < 0$ and $b > 0$, according to Theorem 4.1 given in [39], the COVID-19 infection model (3) doesn't exhibit the backward bifurcation phenomenon at $R_{0_c} = 1$. Thus, we can have the next conclusion.

Theorem 7. *The unique EE, E_c^*, of system (3) is GAS if $R_{0_c} > 1$.*

The appearance of forward/transcritical bifurcation indicates that having $R_{0_c} < 1$, is a necessary and possibly sufficient condition to control the load of the disease from the populations.

3.2. TB sub-model

By making $I_c(t) = R_c(t) = I_{cL}(t) = I_{tc}(t) = 0$ in system (1), we get the TB sub-model:

$$\begin{cases} \dot{S} = \Lambda - (\mu + \lambda_t) S, \\ \dot{L} = \lambda_t S + \varphi \lambda_t R_t - (\phi_t + r_L + \mu) L, \\ \dot{I}_t = \phi_t L - (r_t + \delta_2 + \mu) I_t, \\ \dot{R}_t = r_L L + r_t I_t - (\varphi \lambda_t + \mu) R_t, \end{cases} \tag{10}$$

where $\lambda_t = \dfrac{\beta_t I_t}{N}$ with $N(t) = S(t) + L(t) + I_t(t) + R_t(t)$.

Theorem 8. *Given the initial condition (2), solutions of the TB sub-model (10) remain positive for all time $t > 0$ and the biologically feasible region*

$$\Omega_T = \left\{ (S, L, I_t, R_t) \in \mathbb{R}^4_+ : N(t) \leq \frac{\Lambda}{\mu} \right\},$$

is positively invariant and globally attracting for system (10).

Proof. Adding the right hand side of the TB sub-model (10), the total population satisfy

$$\dot{N}(t) = \Lambda - \mu N - \delta_2 I_t \leq \Lambda - \mu N. \tag{11}$$

Note that, from the initial values (2), we have $N(0) \geq 0$. Hence, for every finite time $t > 0$, the total population is non-negative and bounded. Indeed, the differential equation (11) gives us:

$$N(t) \leq \frac{\Lambda}{\mu},$$

as $t \longrightarrow +\infty$. Hence, the region of definition for system (10) is

$$\Omega_T = \left\{ (S, L, I_t, R_t) \in \mathbb{R}^4_+ : N(t) \leq \frac{\Lambda}{\mu} \right\},$$

and it is positively invariant as well as attracts the solution starting in Ω_T. Thus, it is sufficient to study the TB sub-model (10) dynamics in Ω_T. □

3.2.1. Basic reproduction number for TB sub-model

The DFE point of the TB sub-model (10) is obtained when $L = I_t = 0$ and is given by

$$E_t^0 = (S^0, L^0, I_t^0, R_t^0) = \left(\frac{\Lambda}{\mu}, 0, 0, 0 \right).$$

Following the approach in [37], and considering the infected compartments $x = (L, I_t)^T$, system (10) rewritten as

$$\dot{x} = \mathcal{F}(x) - \mathcal{V}(x),$$

where

$$\mathcal{F} = \begin{bmatrix} \beta_t \dfrac{(S + \varphi R_t) I_t}{N} \\ 0 \end{bmatrix} \quad \text{and} \quad \mathcal{V} = \begin{bmatrix} (\phi_t + r_L + \mu) L \\ -\phi_t L + (r_t + \delta_2 + \mu) I_t \end{bmatrix}.$$

Hence, the corresponding Jacobian matrices evaluated at E_t^0 are given as

$$F = \begin{bmatrix} 0 & \beta_t \\ 0 & 0 \end{bmatrix} \quad \text{and} \quad V = \begin{bmatrix} \phi_t + r_L + \mu & 0 \\ -\phi_t & r_t + \delta_2 + \mu \end{bmatrix}.$$

As a result we obtain

$$V^{-1} = \begin{bmatrix} \dfrac{1}{\phi_t + r_L + \mu} & 0 \\ \dfrac{\phi_t}{(\phi_t + r_L + \mu)(r_t + \delta_2 + \mu)} & \dfrac{1}{r_t + \delta_2 + \mu} \end{bmatrix}.$$

Thus, the next generation matrix is provided by

$$FV^{-1} = \begin{bmatrix} \dfrac{\beta_t \phi_t}{(\phi_t + r_L + \mu)(r_t + \delta_2 + \mu)} & \dfrac{\beta_t}{r_t + \delta_2 + \mu} \\ 0 & 0 \end{bmatrix}.$$

The dominant eigenvalue of FV^{-1} is the basic reproduction number for TB sub-model, i.e.,

$$R_{0_t} = \frac{\beta_t \phi_t}{(\phi_t + r_L + \mu)(r_t + \delta_2 + \mu)}. \tag{12}$$

Next, we examine the local and global asymptotic stability of the DFE, E_t^0, of TB sub-model (10), to determine if the small deviations from the equilibrium point will increase or decrease with time.

3.2.2. Disease-free equilibrium and its stability analysis

Theorem 9. *The TB sub-model* (10) *has a LAS DFE,* E_t^0, *whenever* $R_{0_t} < 1$, *and unstable otherwise.*

Proof. First, let as linearize the system (10) at DFE (E_t^0) to get:

$$J_{E_t^0} = \begin{pmatrix} -\mu & 0 & -\beta_t & 0 \\ 0 & -k_1 & \beta_t & 0 \\ 0 & \phi_t & -k_2 & 0 \\ 0 & r_L & r_t & -\mu \end{pmatrix},$$

where

$$k_1 = \phi_t + r_L + \mu \quad \text{and} \quad k_2 = r_t + \delta_2 + \mu. \tag{13}$$

It is obvious that $\lambda_1 = -\mu = \lambda_4$ are the two negative eigenvalues of $J_{E_t^0}$. The remaining eigenvalues of $J_{E_t^0}$ are obtained from the block matrix

$$J_{1E_t^0} = \begin{pmatrix} -k_1 & \beta_t \\ \phi_t & -k_2 \end{pmatrix},$$

and they are the roots of

$$P(\lambda) = \lambda^2 + a_1\lambda + a_2 = 0, \tag{14}$$

where

$$a_1 = k_1 + k_2,$$
$$a_2 = k_1k_2(1 - R_{0_t}).$$

It can be clearly seen that, $a_1 > 0$ and $a_2 > 0$ for $R_{0_t} < 1$. Again, applying Routh-Hurwitz stability criterion [40,41], the characteristic polynomial (14) have the roots with negative real part, if $R_{0_t} < 1$. If $R_{0_t} > 1$, then $a_3 < 0$ and the equilibrium E_t^0 becomes unstable. Hence, the DFE E_t^0 of the TB sub-model (10) is LAS for $R_{0_t} < 1$. □

Theorem 10. ***(Global stability of DFE:)*** *For $R_{0_t} < 1$, the DFE of the TB sub-model (10) is GAS.*

Proof. Define the Lyapunov function

$$V = k_2L + \beta_t I_t,$$

where k_1 and k_2 are given in (13).

The time derivative of V becomes

$$\begin{aligned}
\dot{V} &= k_2\dot{L} + \beta_t\dot{I}_t \\
&= k_2[\lambda_t S + \varphi\lambda_t R_t - k_1 L] + \beta_t[\phi_t L - k_2 I_t] \\
&= k_2\left[\frac{\beta_t I_t}{N}[S + \varphi R_t] - k_1 L\right] + \beta_t[\phi_t L - k_2 I_t] \\
&\le k_2\left[\frac{\beta_t I_t}{N}N - k_1 L\right] + \beta_t[\phi_t L - k_2 I_t] \\
&= \beta_t\phi_t L - k_1k_2 L \\
&= k_1k_2 L\,(R_{0_t} - 1) \\
&\le 0, \text{ for } R_{0_t} \le 1.
\end{aligned}$$

It can be seen that $\dot{V} \le 0$ for $R_{0_t} \le 1$, with $\dot{V} = 0$ if and only if $L = I_t = 0$. Substituting $(L, I_t) = (0, 0)$ into (10) shows that $S \longrightarrow \frac{\Lambda}{\mu}$ as $t \longrightarrow \infty$. Therefore, the largest compact invariant set in $\{(S, L, I_t, R_t) \in \Omega_T : \dot{V} = 0\}$ is E_t^0 and using LaSalle's invariance principle, E_t^0 is globally asymptotically stable in Ω_T for $R_{0_t} \le 1$. □

3.2.3. Existence and stability of the endemic equilibrium of the TB sub-model

In this subsection, we determine the non zero point for all population components in the TB sub-model.

Theorem 11. *The TB sub-model (10) has only one EE whenever $R_{0_t} > 1$.*

Proof. To proof the theorem, we proceed as follows by solving succeeding system of equations:

$$\begin{aligned}
&\Lambda-(\mu+\lambda_t^*)S^*=0\\
&\lambda_t^*S^*+\varphi\lambda_t^*R_t^*-k_1L^*=0\\
&\phi_tL^*-k_2I_t^*=0\\
&r_LL^*+r_tI_t^*-(\mu+\varphi\lambda_t^*)R_t^*=0,
\end{aligned}\tag{15}$$

where $\lambda_t^*=\dfrac{\beta_tI_t^*}{N^*}=\dfrac{\beta_tI_t^*}{S^*+L^*+I_t^*+R_t^*}$ and k_1,k_2 are given in (13).

A few algebraic calculations later, from equation (15), one can get

$$\begin{aligned}
S^*&=\frac{\Lambda}{\lambda_t^*+\mu},\\
L^*&=\frac{\Lambda k_2\lambda_t^*(\varphi\lambda_t^*+\mu)}{(\lambda_t^*+\mu)(\varphi\lambda_t^*[\mu k_2+\phi_t(\delta_2+\mu)]+\mu k_1k_2)},\\
I_t^*&=\frac{\Lambda\phi_t\lambda_t^*(\varphi\lambda_t^*+\mu)}{(\lambda_t^*+\mu)(\varphi\lambda_t^*[\mu k_2+\phi_t(\delta_2+\mu)]+\mu k_1k_2)},\\
R_t^*&=\frac{\Lambda\lambda_t^*(r_Lk_2+r_t\phi_t)}{(\lambda_t^*+\mu)(\varphi\lambda_t^*[\mu k_2+\phi_t(\delta_2+\mu)]+\mu k_1k_2)},
\end{aligned}\tag{16}$$

where

$$\lambda_t^*=\frac{\beta_tI_t^*}{S^*+L^*+I_t^*+R_t^*}.\tag{17}$$

Note that

$$\beta_tI_t^*=\frac{\beta_t\Lambda\phi_t\lambda_t^*(\varphi\lambda_t^*+\mu)}{(\lambda_t^*+\mu)(\varphi\lambda_t^*[\mu k_2+\phi_t(\delta_2+\mu)]+\mu k_1k_2)}.\tag{18}$$

Also, using equation (16) we have

$$S^*+L^*+I_t^*+R_t^*=\frac{\Lambda}{\lambda_t^*+\mu}+\frac{\Lambda\lambda_t^*(\varphi\lambda_t^*+\mu)}{(\lambda_t^*+\mu)(\varphi\lambda_t^*[\mu k_2+\phi_t(\delta_2+\mu)]+\mu k_1k_2)}\left[k_2+\phi_t+r_Lk_2+r_t\phi_t\right].$$

This implies

$$S^*+L^*+I_t^*+R_t^*=\Lambda\frac{(\varphi\lambda_t^*[\mu k_2+\phi_t(\delta_2+\mu)]+\mu k_1k_2)+\lambda_t^*(\varphi\lambda_t^*+\mu)(k_2+\phi_t+r_Lk_2+r_t\phi_t)}{(\lambda_t^*+\mu)(\varphi\lambda_t^*[\mu k_2+\phi_t(\delta_2+\mu)]+\mu k_1k_2)}.\tag{19}$$

Substituting (18) and (19) into (17), we have

$$\lambda_t^*=\frac{\phi_t\beta_t\lambda_t^*(\varphi\lambda_t^*+\mu)}{(\varphi\lambda_t^*[\mu k_2+\phi_t(\delta_2+\mu)]+\mu k_1k_2)+\lambda_t^*(\varphi\lambda_t^*+\mu)(k_2+\phi_t+r_Lk_2+r_t\phi_t)}.$$

This gives us

$$\lambda_t^*=0\quad\text{or}\quad\varphi\lambda_t^*[\mu k_2+\phi_t(\delta_2+\mu)]+\mu k_1k_2+\lambda_t^*(\varphi\lambda_t^*+\mu)(k_2+\phi_t+r_Lk_2+r_t\phi_t)-\phi_t\beta_t(\varphi\lambda_t^*+\mu)=0.$$

Here, $\lambda_t^*=0$ gives the DFE point. From the second equation we obtain

$$A(\lambda_t^*)^2+B\lambda_t^*+C=0,\tag{20}$$

where

$$\begin{aligned}
A&=\varphi[k_2+\phi_t+(r_Lk_2+r_t\phi_t)]\\
B&=\varphi[\mu r_t+k_1k_2(1-R_{0_t})]+\mu[k_2+\phi_t+(r_Lk_2+r_t\phi_t)]\\
C&=\mu k_1k_2(1-R_{0_t}).
\end{aligned}\tag{21}$$

As it is observed from (21), $B > 0$ and $C > 0$ for $R_{0_t} < 1$. This implies that there does no positive root(s) of (20) exists. For $R_{0_t} > 1$, we have that $C < 0$, and B either positive or negative. This implies the existence of a unique positive root of (20). □

3.2.4. Bifurcation analysis

By using the center manifold theory described in [39], the global stability of the TB sub-model (10) is investigated using the same technique as in Section 3.1. It is first necessary to simplify and change variables in order to apply this theory.

Denoting $x = (x_1, x_2, x_3, x_4)^T = (S, L, I_t, R_t)^T$, the infection model (10) can be altered to take the form $\frac{dx}{dt} = f(x)$, as follows

$$\begin{cases} \frac{dx_1}{dt} = f_1(x) = \Lambda - \beta_t \frac{x_1 x_3}{x_1 + x_2 + x_3 + x_4} - \mu x_1, \\ \frac{dx_2}{dt} = f_2(x) = \beta_t \frac{x_1 x_3}{x_1 + x_2 + x_3 + x_4} + \beta_t \frac{\varphi x_3 x_4}{x_1 + x_2 + x_3 + x_4} - (\phi_t + r_L + \mu) x_2, \\ \frac{dx_3}{dt} = f_3(x) = \phi_t x_2 - (r_t + \delta_2 + \mu) x_3, \\ \frac{dx_4}{dt} = f_4(x) = r_L x_2 + r_t x_3 - \beta_t \frac{\varphi x_3 x_4}{x_1 + x_2 + x_3 + x_4} - \mu x_4. \end{cases} \tag{22}$$

By selecting β_t^* as the bifurcation parameter and R_{0_t} is set to 1, we get

$$\beta_t = \beta_t^* = \frac{(\phi_t + r_L + \mu)(r_t + \delta_2 + \mu)}{\phi_t}.$$

Given below is the linearized matrix for system (22) at E_t^0 and $\beta_t = \beta_t^*$.

$$J_{(E_t^0, \beta_t^*)} = \begin{pmatrix} -\mu & 0 & -\beta_t^* & 0 \\ 0 & -(\phi_t + r_L + \mu) & \beta_t^* & 0 \\ 0 & \phi_t & -(r_t + \delta_2 + \mu) & 0 \\ 0 & r_L & r_t & -\mu \end{pmatrix}.$$

Clearly, $\lambda_1 = -\mu = \lambda_4$ are negative. The rest are obtained from

$$\lambda^2 + (\phi_t + r_L + r_t + \delta_2 + 2\mu)\lambda = 0,$$

which are $\lambda_2 = 0$ and $\lambda_3 = -(\phi_t + r_L + r_t + \delta_2 + 2\mu)$. This implies, at $\beta_t = \beta_t^*$, the DFE, E_t^0, is a non-hyperbolic.

Next, we proceed the method as follows. Representing the right eigenvector of the system (22) by $w = (w_1, w_2, w_3, w_4)^T$ and solving for

$$J_{(E_t^0, \beta_t^*)} \cdot w = 0,$$

we get the right eigenvectors

$$w_1 = -\frac{k_1 k_2}{r_L k_2 + r_t \phi_t} w_4, \quad w_2 = \frac{\mu k_2}{r_L k_2 + r_t \phi_t} w_4, \quad w_3 = \frac{\mu \phi_t}{r_L k_2 + r_t \phi_t} w_4, \quad w_4 = w_4 > 0.$$

Similarly, representing the left eigenvector of the system (22) by $v = (v_1, v_2, v_3, v_4)$ and solving for

$$v \cdot J_{(E_t^0, \beta_t^*)} = 0,$$

we get the left eigenvectors

$$v_1 = 0, \quad v_4 = 0, \quad v_2 = \frac{\phi_t}{\phi_t + r_L + \mu} v_3, \quad v_3 = v_3 > 0.$$

Both eigenvectors must fulfill:

$$v \cdot w = v_3 w_4 \left(\frac{r_t + \delta_2 + \mu}{\phi_t + r_L + \mu} + 1 \right) \frac{\mu \phi_t}{r_L(\phi_t + r_L + \mu) + r_t \phi_t} = 1.$$

Direction of the bifurcation: The coefficients of the bifurcation at E_t^0 are given as:

$$a = \sum_{k,i,j=1}^{4} v_k w_i w_j \frac{\partial^2 f_k}{\partial x_i \partial x_j}(E_t^0, \beta_t^*)$$

$$b = \sum_{k,i=1}^{4} v_k w_i \frac{\partial^2 f_k}{\partial x_i \partial \beta_t}(E_t^0, \beta_t^*).$$

Since $v_1 = v_4 = 0$, we do not need the derivatives of f_1 and f_4. Also, the second-order partial derivatives of f_3 are all zero. Therefore, all that is required are the partial derivatives of f_2, where

$$f_2 = \frac{\beta_t x_1 x_3}{x_1 + x_2 + x_3 + x_4} + \frac{\beta_t \varphi x_3 x_4}{x_1 + x_2 + x_3 + x_4} - (\phi_t + r_L + \mu)x_2.$$

Thus, we obtain the following nonzero 2nd order partial derivatives of f_2 at (E_t^0, β_t^*):

$$\frac{\partial^2 f_2}{\partial x_3 \partial x_2}(E_t^0, \beta_t^*) = \frac{\partial^2 f_2}{\partial x_3 \partial x_4}(E_t^0, \beta_t^*) = -\beta_t^* \frac{\mu}{\Lambda}, \quad \frac{\partial^2 f_2}{\partial x_3^2}(E_t^0, \beta_t^*) = -2\beta_t^* \frac{\mu}{\Lambda}, \quad \text{and} \quad \frac{\partial^2 f_2}{\partial x_3 \partial \beta_t}(E_t^0, \beta_t^*) = 1.$$

Now, we obtain

$$\begin{aligned} a &= \sum_{k,i,j=1}^{4} v_k w_i w_j \frac{\partial^2 f_k}{\partial x_i \partial x_j}(E_t^0, \beta_t^*) \\ &= v_2 \left[2w_3 w_2 \frac{\partial^2 f_2}{\partial x_3 \partial x_2}(E_t^0, \beta_t^*) + 2w_3 w_4 \frac{\partial^2 f_2}{\partial x_3 \partial x_4}(E_t^0, \beta_t^*) + w_3^2 \frac{\partial^2 f_2}{\partial x_3^2}(E_t^0, \beta_t^*) \right] \\ &= -2\beta_t^* \frac{\mu}{\Lambda}(w_2 + w_3 + \varphi w_4) v_2 w_3 < 0. \end{aligned}$$

Further, the bifurcation constant b is provided by

$$\begin{aligned} b &= \sum_{k,i=1}^{4} v_k w_i \frac{\partial^2 f_k}{\partial x_i \partial \beta_t}(E_t^0, \beta_t^*) \\ &= v_2 w_3 \frac{\partial^2 f_2}{\partial x_3 \partial \beta_t}(E_t^0, \beta_t^*) \\ &= v_2 w_3 > 0. \end{aligned}$$

Thus, $a < 0$ and $b > 0$ at $\beta_t = \beta_t^*$. Therefore, Theorem 4.1 in [39] implies the TB sub-model (10) doesn't demonstrate the backward bifurcation conditions at $R_{0_t} = 1$ and thus, the coexistence of a stable DFE with a stable EE is not possible. As a result, the next conclusion follows.

Theorem 12. *The unique EE (E_t^0) of the TB sub-model (10) is GAS if $R_{0_t} > 1$.*

3.3. COVID-19-TB co-infection model

This section presents the analysis of the full TB-COVID-19 system given in (1). The region of invariance for model (1) is given by

$$\Omega_{CT} = \Omega_C \times \Omega_T,$$

where Ω_C and Ω_T, respectively are the invariant region for the sub-models (3) and (10). Following the same approach in [23,34,35], one can show that for any time $t \geq 0$, the solution of model (1) with non-negative initial values (2) remains non-negative. Moreover, from permanence theory [33], all solutions of system (1) at the boundary of Ω_{CT} enter the interior of Ω_{CT}. Hence, Ω_{CT} is positively invariant as well as attracts the flow generated by model (1).

3.3.1. Stability analysis of the disease-free equilibrium

The TB-COVID-19 model (1) has a DFE which is provided by

$$E^0 = (S^0, L^0, I_c^0, I_t^0, I_{cL}^0, I_{tc}^0, R_t^0, R_c^0) = \left(\frac{\Lambda}{\mu}, 0, 0, 0, 0, 0, 0, 0 \right).$$

As shown in the previous sections, one can apply the next generation method and obtain the basic reproduction number of COVID-19 and TB co-infection model (1) as follows:

$$R_0 = \max \left\{ R_{0_c}, R_{0_t} \right\},$$

where R_{0_c} and R_{0_t} are as given in (6) and (12), respectively. From this we conclude that the co-infection dynamics will be in control of by the disease that have highest reproductive number.

Theorem 13. *For $R_0 < 1$, the DFE, E^0, of the system (1) is LAS, and unstable otherwise.*

Proof. The linearized matrix of system (1) at E^0, is given as

$$J_{E^0} = \begin{pmatrix} -\mu & 0 & -\beta_c(1-\kappa\rho) & -\beta_t & -\beta_c\tau(1-\kappa\rho) & -\beta_c\tau(1-\kappa\rho)-\beta_t & 0 & 0 \\ 0 & -k_1 & 0 & \beta_t & \eta_L & \beta_t & 0 & 0 \\ 0 & 0 & \beta_c(1-\kappa\rho)-k_2 & 0 & \beta_c\tau(1-\kappa\rho) & \alpha_c+\beta_c\tau(1-\kappa\rho) & 0 & 0 \\ 0 & \phi_t & 0 & -k_3 & 0 & \theta & 0 & 0 \\ 0 & 0 & 0 & 0 & -k_4 & 0 & 0 & 0 \\ 0 & 0 & 0 & 0 & \eta_c & -k_5 & 0 & 0 \\ 0 & 0 & r_c & 0 & 0 & 0 & -\mu & 0 \\ 0 & r_L & 0 & r_t & 0 & 0 & 0 & -\mu \end{pmatrix},$$

where

$$k_1 = \phi_t + r_L + \mu,\ k_2 = r_c + \delta_1 + \mu,\ k_3 = r_t + \delta_2 + \mu,\ k_4 = \eta_c + \eta_L + \mu,\ k_5 = \alpha_c + \theta + \delta_3 + \mu. \tag{23}$$

Note that, $\lambda_1 = -\mu$, $\lambda_7 = -\mu$ and $\lambda_8 = -\mu$ are the eigenvalues of J_{E^0}. The remaining eigenvalues of J_{E^0} are obtained from the block matrix

$$J_{1E^0} = \begin{pmatrix} -k_1 & 0 & \beta_t & \eta_L & \beta_t \\ 0 & \beta_c(1-\kappa\rho)-k_2 & 0 & \beta_c\tau(1-\kappa\rho) & \alpha_c+\beta_c\tau(1-\kappa\rho) \\ \phi_t & 0 & -k_3 & 0 & \theta \\ 0 & 0 & 0 & -k_4 & 0 \\ 0 & 0 & 0 & \eta_c & -k_5 \end{pmatrix}.$$

The eigenvalues of J_{1E^0} are obtained from the following block matrices:

$$J_{2E^0} = \begin{pmatrix} -k_1 & 0 & \beta_t \\ 0 & \beta_c(1-\kappa\rho)-k_2 & 0 \\ \phi_t & 0 & -k_3 \end{pmatrix} \quad \text{and} \quad J_{3E^0} = \begin{pmatrix} -k_4 & 0 \\ \eta_c & -k_5 \end{pmatrix}.$$

Clearly, $\lambda_5 = -k_4$ and $\lambda_6 = -k_5$ are the eigenvalues of J_{3E^0} (which are negative) and the eigenvalues for J_{2E^0} are obtained from

$$\left(k_2\left[R_{0_c} - 1\right] - \lambda\right)\left(\lambda^2 + a_1\lambda + a_2\right) = 0, \tag{24}$$

where

$$a_1 = k_1 + k_2$$
$$a_2 = k_1k_2[1 - R_{0_t}].$$

From (24), we obtain the eigenvalues with negative real parts, when $R_0 = \max\left\{R_{0_c}, R_{0_t}\right\} < 1$. Hence, E^0 is LAS if $R_0 < 1$ and unstable otherwise. □

In the following theorem, the GAS of DFE for model (1) is performed following the approach in [42].

Theorem 14. *If $R_0 < 1$, the DFE (E^0) of the TB-COVID-19 model (1) is globally asymptotically stable in Ω_{CT}.*

Proof. To proof the theorem, we first rewrite the co-dynamics model (1) in the form

$$\frac{d\mathcal{X}}{dt} = F(\mathcal{X}, \mathcal{Y}),$$
$$\frac{d\mathcal{Y}}{dt} = G(\mathcal{X}, \mathcal{Y}), \text{ with } G(\mathcal{X}, 0) = 0,$$

where $\mathcal{X} = (S, R_c, R_t) \in \mathbb{R}^3_+$ denotes non-infected compartments, and $\mathcal{Y} = (L, I_c, I_t, I_{cL}, I_{tc}) \in \mathbb{R}^5_+$ denotes the infected compartments. Then we have to check the following two requirements.

(H_1) $\frac{d\mathcal{X}}{dt} = F(\mathcal{X}, 0)$, $\mathcal{X}^*$ is GAS, where $F(\mathcal{X}^*, 0) = 0$.
(H_2) $G(\mathcal{X}, \mathcal{X}) = B\mathcal{Y} - \tilde{G}(\mathcal{X}, \mathcal{Y})$, $\tilde{G}(\mathcal{X}, \mathcal{Y}) > 0$ for $(\mathcal{X}, \mathcal{Y}) \in \Omega_{CT}$, where $B = D_{\mathcal{Y}}G(\mathcal{X}^*, 0)$ is an M-matrix.

For the co-dynamics model (1), we have

$$\frac{d\mathcal{X}}{dt} = \begin{pmatrix} \Lambda - \mu S \\ -\mu R_c \\ -\mu R_t \end{pmatrix} \tag{25}$$

The DFE for the system (25) is given by $\mathcal{X}^* = (\frac{\Lambda}{\mu}, 0, 0)$. The system (25) is globally asymptotically stable around its unique equilibrium point $\mathcal{X}^*$. Indeed, the trajectories $S(t) = \frac{\Lambda}{\mu} + (S(0) - \frac{\Lambda}{\mu})e^{-\mu t}$, $R_c(t) = R_c(0)e^{-\mu t}$ and $R_t(t) = R_t(0)e^{-\mu t}$ satisfies $\lim_{t\longrightarrow\infty} S(t) = \frac{\Lambda}{\mu}$, $\lim_{t\longrightarrow\infty} R_c(t) = 0$ and $\lim_{t\longrightarrow\infty} R_t(t) = 0$, respectively, which implies that the global convergence of the system (25) in Ω_{CT}. Thus, the condition (H_1) is satisfied.

Furthermore, from model (1), we have

$$\frac{dY}{dt} = G(X,Y) = \begin{pmatrix} \lambda_t S + \eta_L I_{cL} + \varphi\lambda_t R_t + \lambda_t R_c - (\lambda_c + \phi_t + r_L + \mu)L \\ \lambda_c S + \alpha_c I_{tc} + \nu\lambda_c R_t - (\omega\lambda_t + r_c + \delta_1 + \mu)I_c \\ \phi_t L + \theta I_{tc} - (\sigma\lambda_c + r_t + \delta_2 + \mu)I_t \\ \lambda_c L + \omega\lambda_t I_c - (\eta_c + \eta_L + \mu)I_{cL} \\ \sigma\lambda_c I_t + \eta_c I_{cL} - (\alpha_c + \theta + \delta_3 + \mu)I_{tc} \end{pmatrix}$$

and we obtain the Metzler Matrix as follows

$$B = D_{\mathcal{Y}} G(\mathcal{X}^*, 0) = \begin{pmatrix} -k_1 & 0 & \beta_t & \eta_L & \beta_t \\ 0 & \beta_c(1-\kappa\rho) - k_2 & 0 & \beta_c\tau(1-\kappa\rho) & \alpha_c + \beta_c\tau(1-\kappa\rho) \\ \phi_t & 0 & -k_3 & 0 & \theta \\ 0 & 0 & 0 & -k_4 & 0 \\ 0 & 0 & 0 & \eta_c & -k_5 \end{pmatrix},$$

where k_1, k_2, k_3, k_4 and k_5 are as in (23).

Now, we have

$$\begin{aligned} \tilde{G}(\mathcal{X}, \mathcal{Y}) &= B\mathcal{Y} - G(\mathcal{X}, \mathcal{Y}) \\ &= \begin{pmatrix} \beta_t(I_t + I_{tc}) - \lambda_t(S + \varphi R_t + R_c) + \lambda_c L \\ \beta_c(1-\kappa\rho)(I_c + \tau(I_{cL} + I_{tc})) - \lambda_c S - \nu\lambda_c R_t + \omega\lambda_t I_c \\ \sigma\lambda_c I_t \\ -\lambda_c L - \omega\lambda_t I_c \\ -\sigma\lambda_c I_t \end{pmatrix}. \end{aligned}$$

Easy observation reveals that $\tilde{G}(\mathcal{X}, \mathcal{Y}) \not\geq 0$, which implies the (H_2) requirement is not met. Thus, the DFE point E^0 may not be globally asymptotically stable. □

Since the phenomenon of backward bifurcation does not occur in both COVID-19 and TB submodels, so is that for the co-infection model [23]. Thus, depending on the occurrence of forward bifurcation in each sub-models, the co-infection model equilibrium points are locally as well as GAS [25].

4. Numerical simulation

To demonstrate the theoretical results, numerical simulations are carried out. Model parameter values and their sources are listed in Table 2 for the numerical simulations.

4.1. Curve fitting

We fitted the model (1) to the COVID-19 data provided by the health authorities in Ethiopia [43] from March 13, 2020, until May 31, 2022. In order to fit the cumulative daily COVID-19 cases, we use model (1) and use the programming language Python (version 3.7) [44]. The cumulative daily COVID-19 cases were obtained from the Ethiopian Public Health Institute (EPHI) [43] and also available online at [45]. The population of Ethiopia is estimated to be $N(0) = 114,963,588$ and the life expectancy (in days) is $\mu = 1/(67.8 \times 365)$ for the year 2021 [46]. We define the initial values for each of the state variables on March 13, 2020 as follows: $L(0) = 200,000$, $I_t(0) = 151,000$, $I_c(0) = 1$, $I_{cL}(0) = 0$, $I_{tc}(0) = 0$, $R_c(0) = 0$ and $R_t(0) = 7000$. From these, we have $S(0) = N(0) - [L(0) + I_c(0) + I_t(0) + I_{cL}(0) + I_{tc}(0) + R_c(0) + R_t(0)]$.

The influx rate, Λ, is calculated from the relation $\Lambda/\mu = N(0)$, and it is obtained $4,645$. Further, we assumed the values of ρ and κ between 0 and 1. For the model fitting, we used $scipy.optimize.curve\_fit$ from Python, see [47] and [48] for more details, that uses non-linear least squares method to fit a function to data. The best fit to the model is portrayed in Fig. 2.

4.2. Simulation results

In this subsection, we validate the local and global asymptotic stability of DFE and EE point of the COVID-19 and TB co-infection model (1). Using the baseline parameter values in Table 2 except $\beta_c = 0.376513$ and $\beta_t = 0.638827$, the associated reproductive numbers

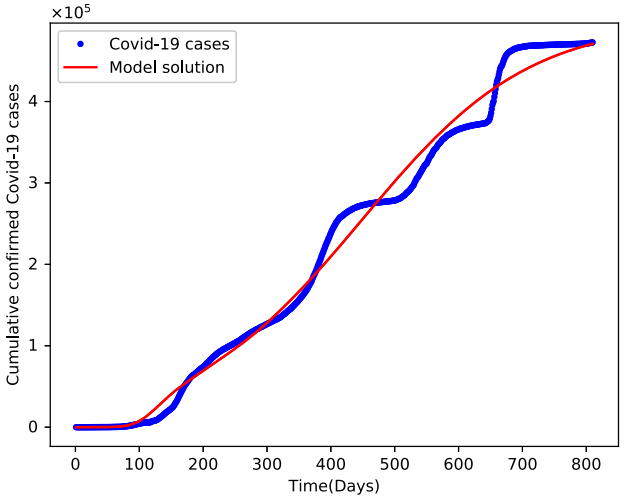

Fig. 2. Model fitting to the cumulative daily COVID-19 cases in Ethiopia, March 13, 2020 – May 31, 2022.

Table 2
Parameters value.

Parameters	Estimated values	References
Λ	4645	Calculated
μ	$1/(67.8\times 365)$	[46]
κ	0.3	Assumed
ρ	0.5	Assumed
β_c	0.506513	Fitted
β_t	0.858827	Fitted
τ	1.007301	Fitted
δ_1	0.001518	Fitted
δ_2	21/100000	[49]
δ_3	0.010398	Fitted
ϕ_t	0.274029	Fitted
r_c	0.324156	Fitted
r_t	0.175492	Fitted
r_L	0.749912	Fitted
ω	1.018125	Fitted
σ	1.009452	Fitted
α_c	0.782631	Fitted
η_c	0.429445	Fitted
η_L	0.932234	Fitted
θ	0.840226	Fitted
ν	1.000108	Fitted
φ	1.002361	Fitted

are obtained as $R_{0_c} = 0.9826$ and $R_{0_t} = 0.9728$, both of which are less than one and hence, $R_0 = \max\left\{R_{0_c}, R_{0_t}\right\}$ is less than unity. From Figs. 3a and 3b, it is evident that the solution trajectories of the infected compartments are moving toward the respective components of the DFE when the basic reproductive number R_0 related to COVID-19 and TB is below one. This figure reveals that, for the basic reproduction number R_0 less than unity, both diseases will die out in the population.

Fig. 4 illustrates the time series plot of the COVID-19 and TB co-infection model using the baseline parameter values described in Table 2, so that its basic reproductive number is exceeds one. As it can be shown in Figs. 4a and 4b, all solution curves are converged to their corresponding components of the EE.

The time series plot for the numerical solutions of the COVID-19 and TB co-infection model (1) using different initial conditions are plotted in Fig. 5. In this case, we use the baseline parameter values described in Table 2, so that its basic reproductive number is exceeds one. The Figures given in 5a, 5b, 5c, and 5d reveal that, for the basic reproduction number R_0 greater than unity, both diseases will persist in the population.

Fig. 6 and Fig. 7 justifies the GAS of DFE (E^0) for COVID-19-TB co-infection model (1). Taking various initial values for infected compartments, each solution curve moves toward the DFE point when $R_0 < 1$ as seen for latent TB, and active TB from Figs. 6a and 6b. Similarly, one can observe the convergence of co-infected individuals to DFE point from Figs. 7a and 7b.

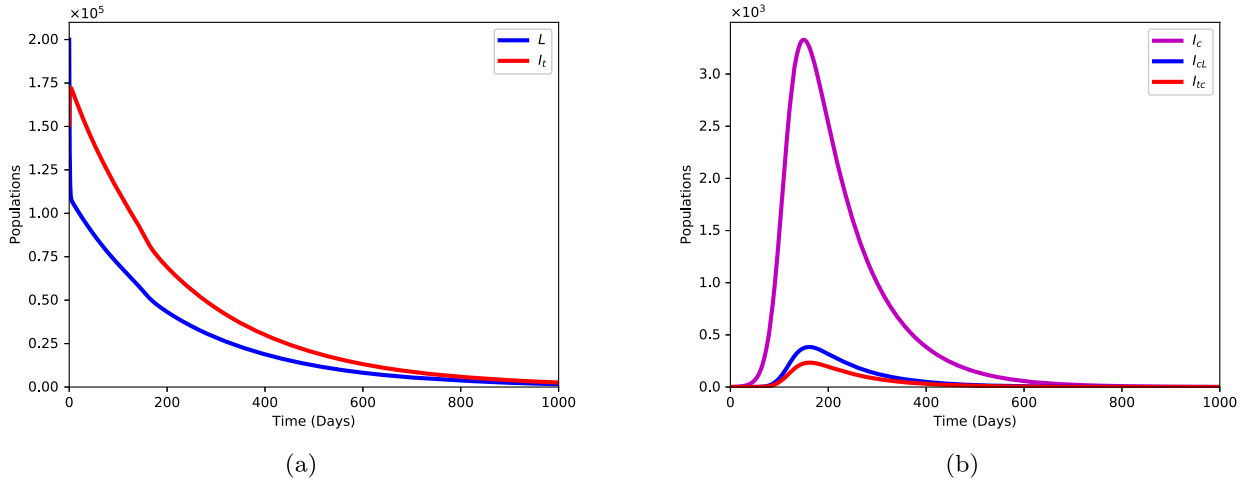

Fig. 3. Simulations showing the local stability of DFE for the model (1). Here $\beta_c = 0.376513$ and $\beta_t = 0.638826$ so that $R_{0_c} = 0.9826 < 1$ and $R_{0_t} = 0.9728 < 1$. All other parameters are as in Table 2.

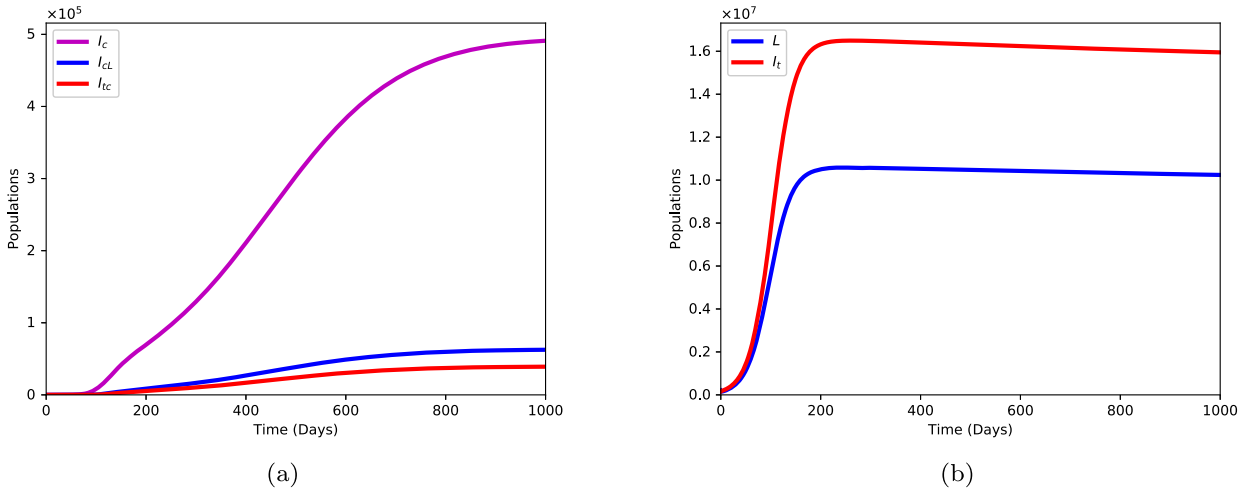

Fig. 4. Simulations showing the convergence of model (1) solution to EE. Here we use the baseline parameter values in Table 2 so that $R_{0_c} = 1.3218 > 1$ and $R_{0_t} = 1.3078 > 1$.

4.2.1. *Impact of COVID-19 contact rate on COVID-19 and TB co-dynamics*

The effects of COVID-19 contact rate (β_c) on the dynamics of infected individuals for model (1) are portrayed in Fig. 8. It is noticeable from Fig. 8a that the number of people who become COVID-19 infected is less when β_c decreases; however, they start increasing for a high values of β_c, due to the increase in COVID-19 contact rate. Moreover, in a similar manner, the COVID-19 contact rate (β_c) has the same effects on the co-infected individuals as described in Figs. 8b and 8c respectively.

4.2.2. *Impact of the fraction of the community applying COVID-19 personal protection measure*

Fig. 9 shows the simulation for various effectiveness of the fraction of the community applying COVID-19 personal protection measure (κ). Simulation of model (1) for the population of COVID-19 infected individuals (I_c), at different values of κ, is portrayed in Fig. 9a. As seen from this figure, increasing the number of communities employing COVID-19 personal protection strategy could significantly reduce the COVID-19 infection from the community. Moreover, a similar trend is observed in Figs. 9b and 9c, revealing that increasing fraction of the community applying COVID-19 personal protection measure could also minimize the difficulty of the co-infections. In comparison with a small number of communities employing COVID-19 personal protection strategy, the result shows that: adopting a high number of communities employing COVID-19 personal protection strategy will minimize the cumulative number of individuals become infected and co-infected with both diseases. In general, increasing the number of communities employing COVID-19 personal protection strategy would results in reduction in the number of individuals that would be confirmed with COVID-19 and co-infected with the two diseases.

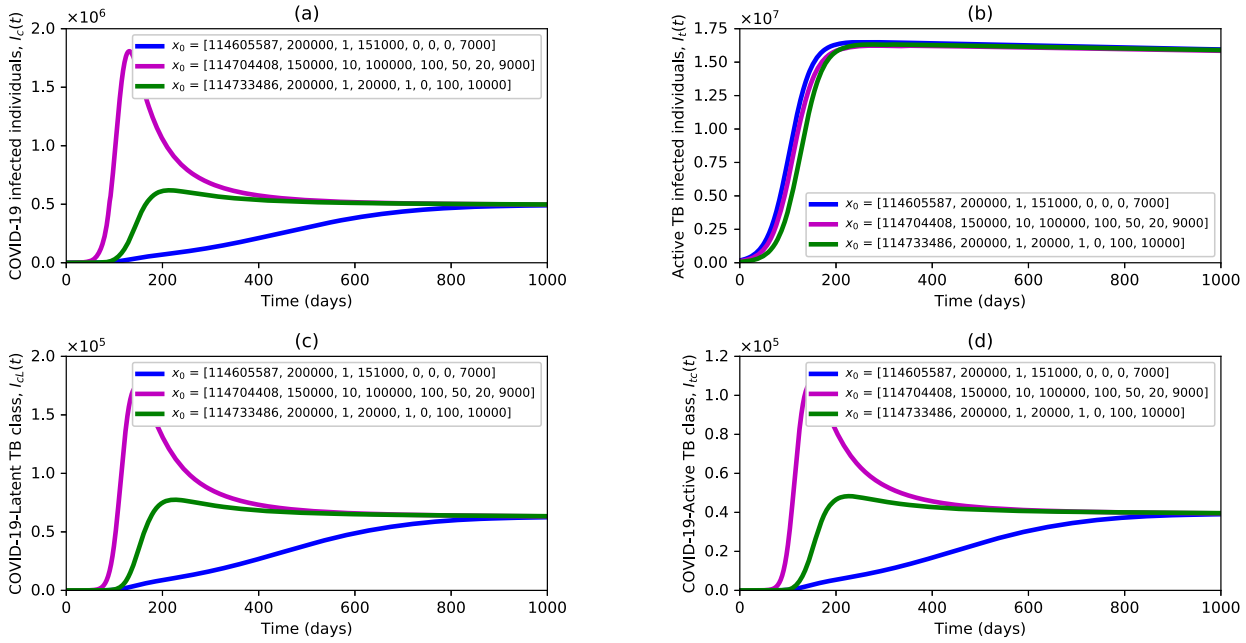

Fig. 5. Simulations of model (1) showing the number of infected and co-infected individuals at various initial values using the parameter values in Table 2 so that $R_{0_c} = 1.3218 > 1$ and $R_{0_t} = 1.3078 > 1$.

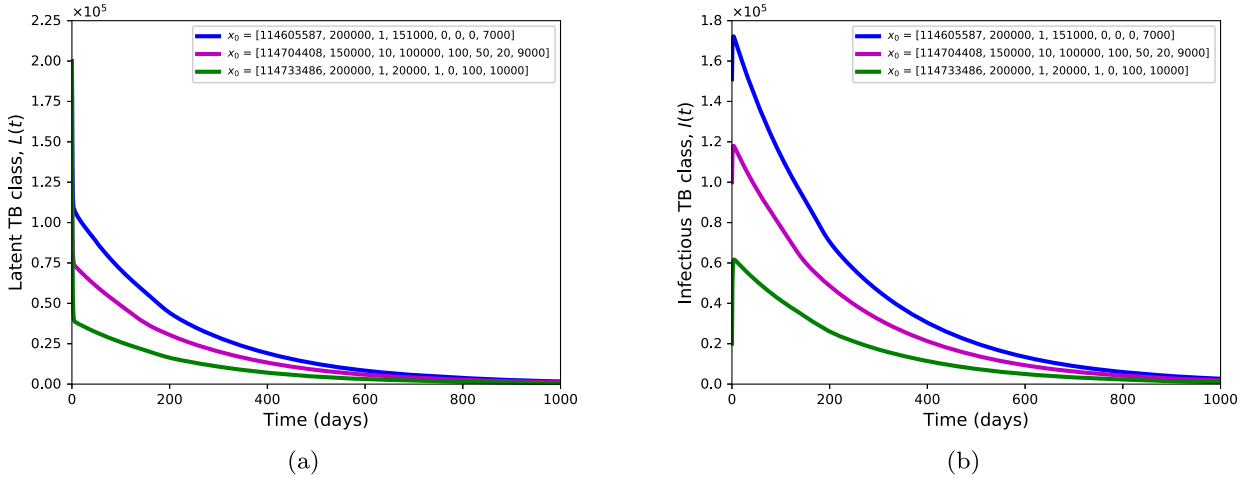

Fig. 6. Simulations of model (1) showing the number of (a) Latent TB and (b) active TB infected individuals at various initial values using parameter values in Table 2 except $\beta_c = 0.376513$ and $\beta_t = 0.638826$ so that $R_{0_c} = 0.9826 < 1$ and $R_{0_t} = 0.9728 < 1$.

4.2.3. *Impact of modification parameter accounting for the infectiousness of individuals contracting COVID-19 due to TB infection*

Fig. 10 depicts the simulation of model (1) for the number of individuals that are infected by COVID-19 (I_c), and having active TB and COVID-19 (I_{tc}), at different values of the modification parameters σ and ν. As shown in Fig. 10a, reducing the possibility of the persons that will contract COVID-19 as a result of active TB would significantly decrease COVID-19 infections in the community. Similar observation is also seen from Fig. 10b in the case of co-infection for COVID-19 and active TB. The simulation results of COVID-19 infected individuals (I_c) at various values of the modification parameter that account relative contagiousness of people contracting COVID-19 after TB recovery, is also represented in Fig. 10c, and it reveals that preventing the possibility of acquiring COVID-19 after TB recovery would also help curb the COVID-19 infection. In contrast, TB lowers the immunity against COVID-19 leading, to increased occurrence of COVID-19 infection.

4.2.4. *Conditions for both diseases to coexist or eradication*

In this subsection, numerical simulations of the co-infection model (1) are performed to ascertain whether the two diseases will co-exist if their respective basic reproduction numbers exceeds one. In Fig. 11, we have represented simulations for the total number

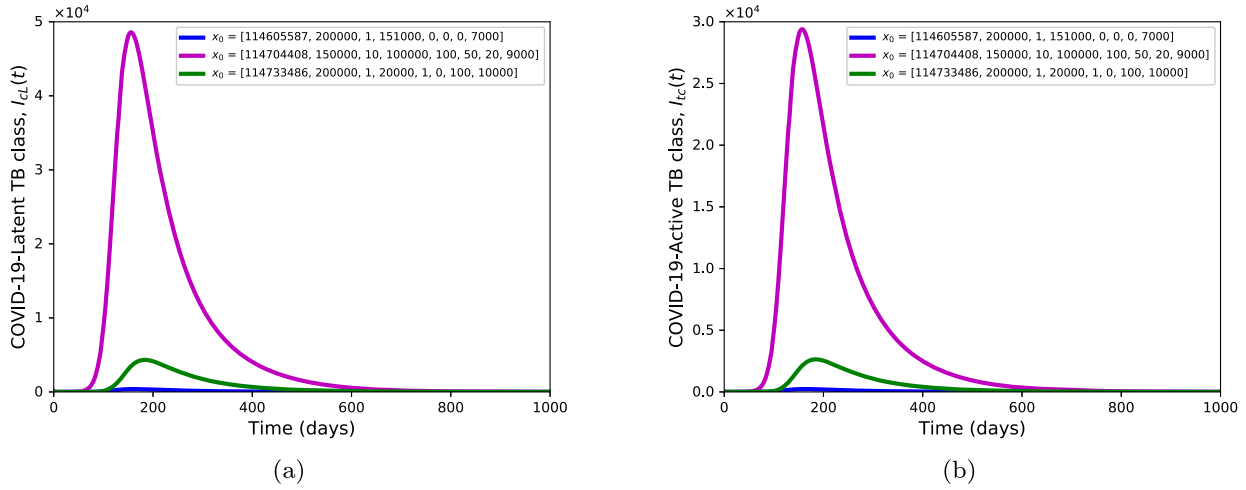

Fig. 7. Simulations of model (1) showing the number of co-infected individuals at various initial values using parameter values in Table 2 except $\beta_c = 0.376513$ and $\beta_t = 0.638826$ so that $R_{0_c} = 0.9826 < 1$ and $R_{0_t} = 0.9728 < 1$.

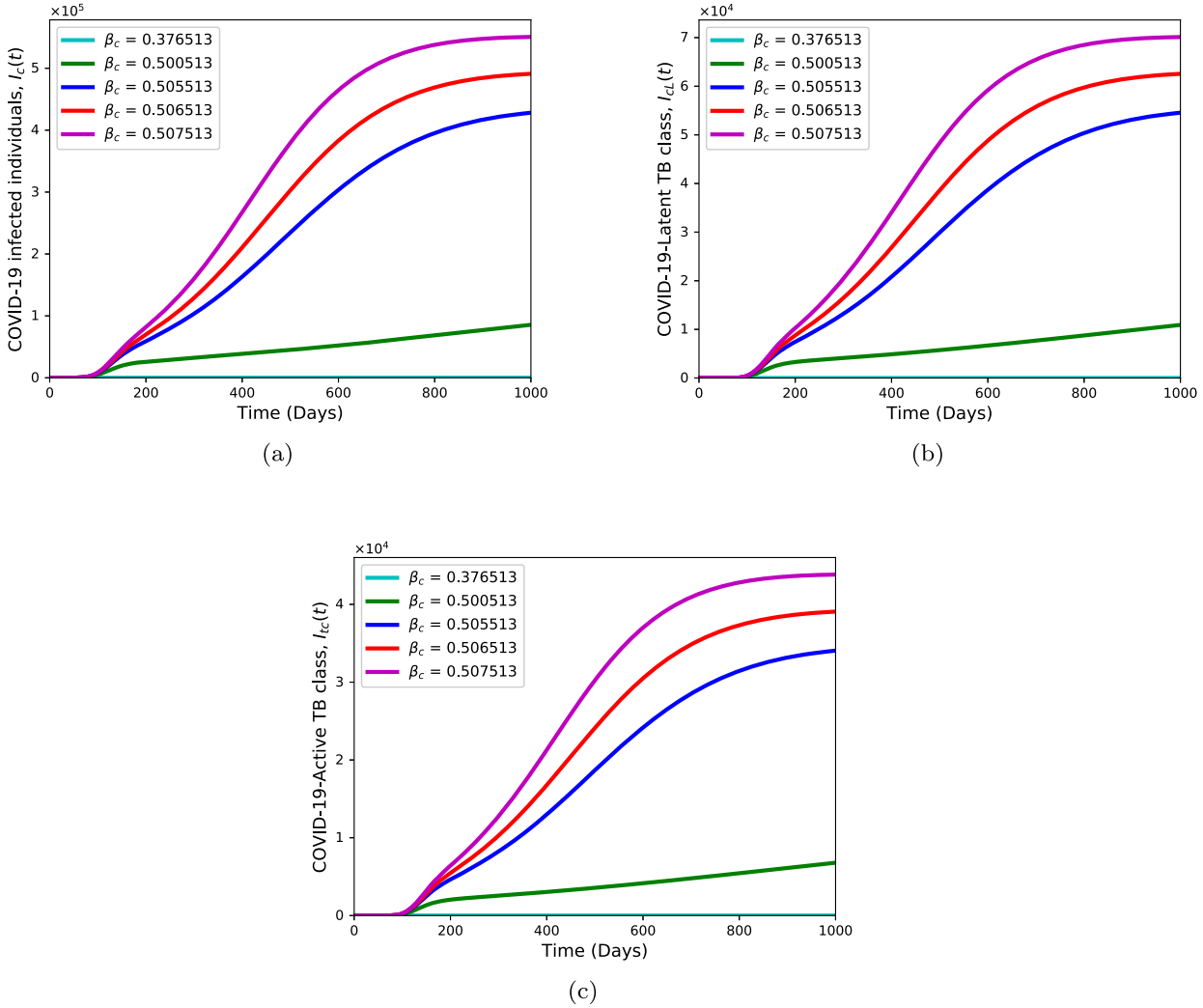

Fig. 8. Simulations of model (1) showing the total number of (a) COVID-19 infected (b) Co-infected class I_{cL} (c) Co-infected class I_{tc} at various values of β_c.

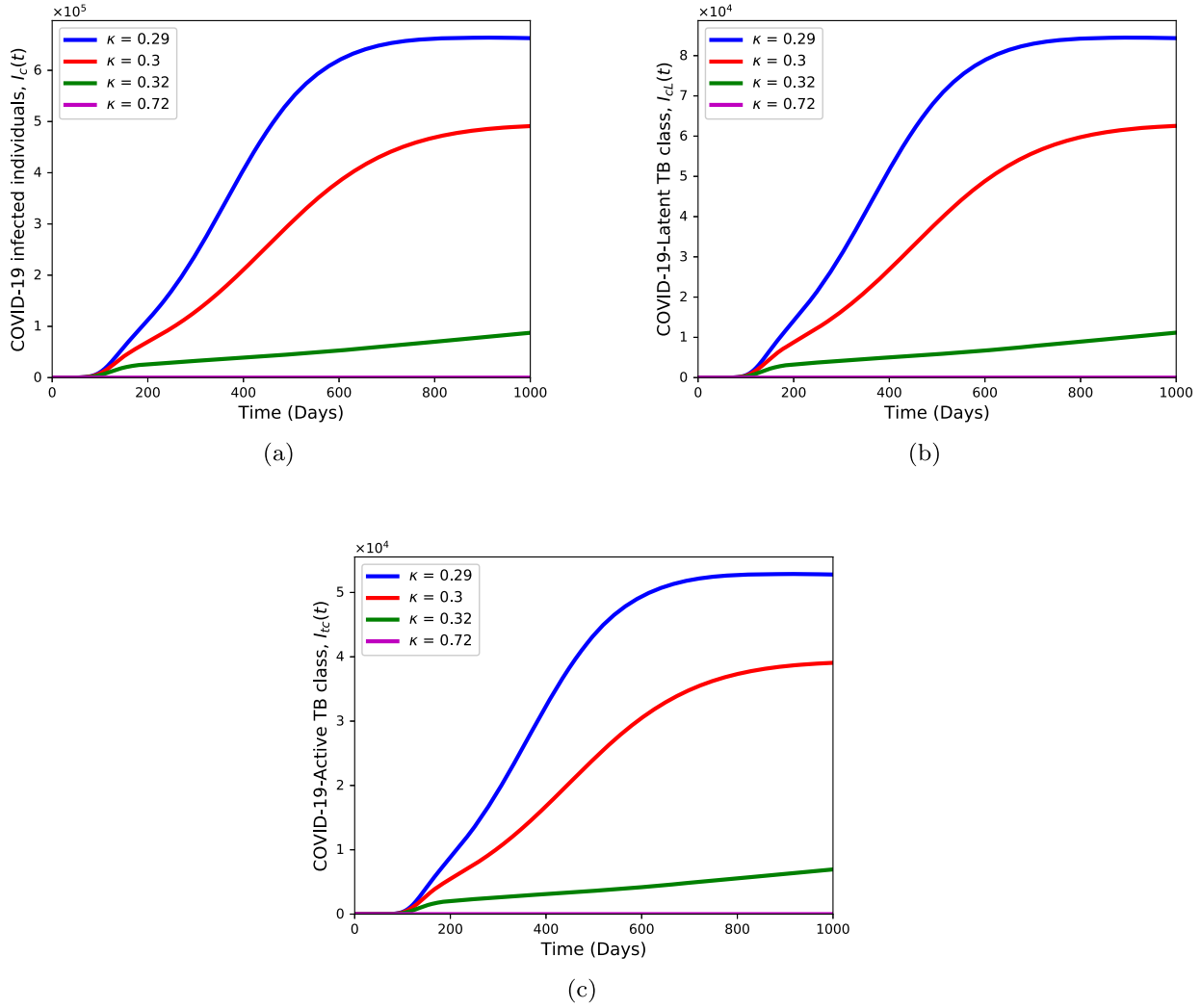

Fig. 9. Simulations of model (1) showing the total number of (a) COVID-19 infected (b) Co-infected class I_{cL} (c) Co-infected class I_{tc} at various values of κ.

of infectious individuals at various initial values for R_{0_c} and R_{0_t} greater than unity. It is observed from this figure, that for higher contact rates of COVID-19 ($\beta_c = 0.506513$) and tuberculosis ($\beta_t = 0.858827$), both COVID-19 and TB will persist in the community.

Fig. 12, depicts the results of the simulations for COVID-19 infected and active TB infected individuals at various initial values for $R_{0_c} < 1$ and $R_{0_t} > 1$. It is revealed here, that for lower contact rate of COVID-19 ($\beta_c = 0.376513$) and higher contact rate of TB ($\beta_t = 0.858827$), COVID-19 will be driven to extinction by TB dominating the population over time.

In Fig. 13, we have depicted the simulation results of infected individuals at various initial values for R_{0_c} and R_{0_t} less than unity. In view of this figure, it is evident that for low TB and COVID-19 contact rates and as a result of increased COVID-19 treatment rates, the two diseases will eventually disappear from the community over time.

The simulation results of the co-infected populations at various initial values for R_{0_c} and R_{0_t} greater than unity are portrayed in Fig. 14. From this figure, it is visualized that, for higher contact rates of COVID-19 ($\beta_c = 0.506513$) and tuberculosis ($\beta_t = 0.858827$), the two diseases will coexist in the community, with COVID-19 and latent TB co-infected dominating the individuals in co-infection class I_{tc}.

5. Conclusions

We proposed a mathematical model with the objective of investigating the dynamics of co-infection for COVID-19 and TB. Basic model characteristics, including the nonnegativity and boundedness of the model solution as well as the invariant region, are provided. Furthermore, for each sub-models equilibrium points, the stability and bifurcation analysis are presented. Particularly, their DFE points are both LAS and GAS for the corresponding reproductive numbers R_{0_c} and R_{0_t} less than unity, unstable otherwise. Besides, the EE of both sub-models existed and its stability analysis were investigated. Consequently, the coexistence equilibrium point of each sub-model is LAS for $R_{0_c} > 1$ and $R_{0_t} > 1$. We have showed that the model undergoes forward bifurcation. From the

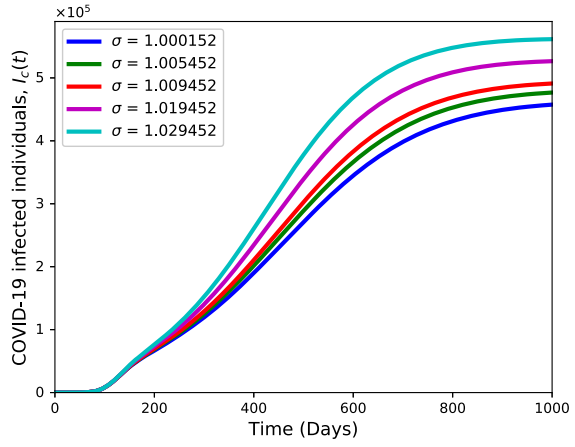

(a)

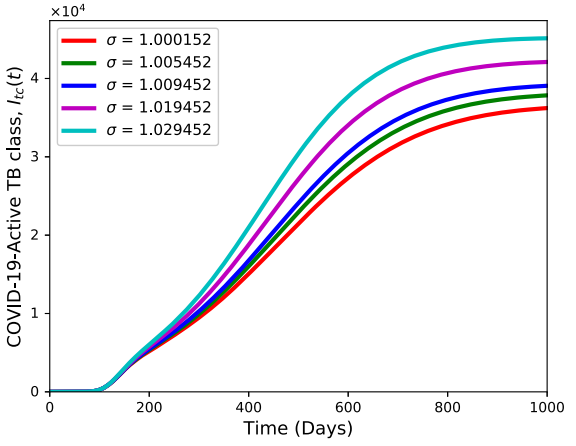

(b)

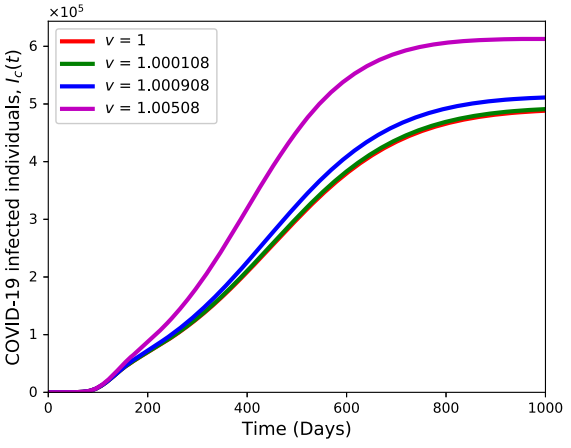

(c)

Fig. 10. The simulations showing (a) COVID-19 infected individuals at different values of σ (b) COVID-19 and active TB co-infected individuals at various values of σ (c) individuals infected by COVID-19 at various values of v.

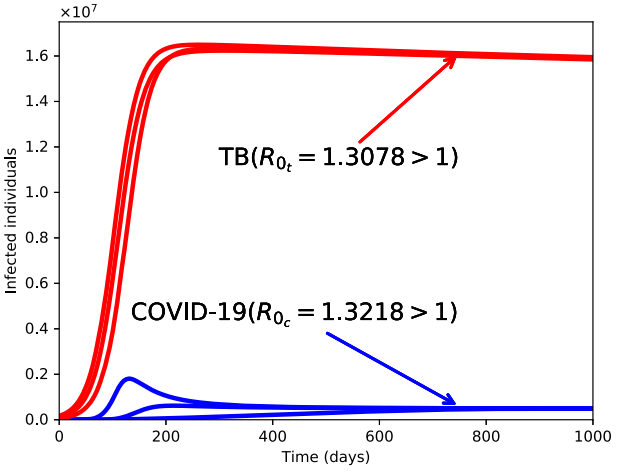

Fig. 11. Simulations of the model (1) with various initial values illustrating the infected class I_t, and I_c. Here, all the values of the parameters are as in Table 2 so that $R_{0_c} = 1.3218 > 1$ and $R_{0_t} = 1.3078 > 1$.

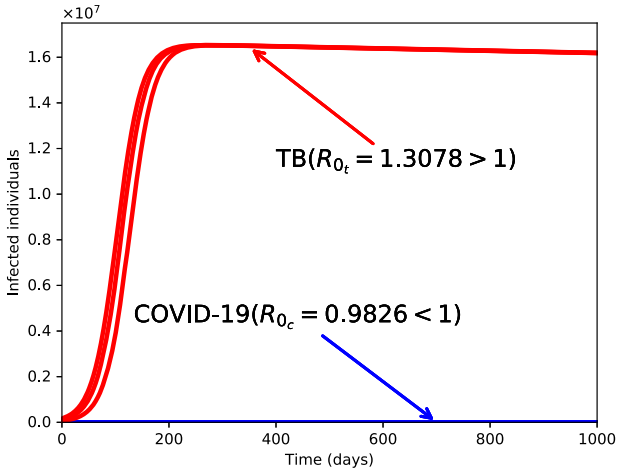

Fig. 12. The simulations illustrating COVID-19, and TB infection at various initial values so that $R_{0_c} = 0.9826 < 1$ and $R_{0_t} = 1.3078 > 1$. Here, all the values of the parameters are as in Table 2 except $\beta_c = 0.376513$.

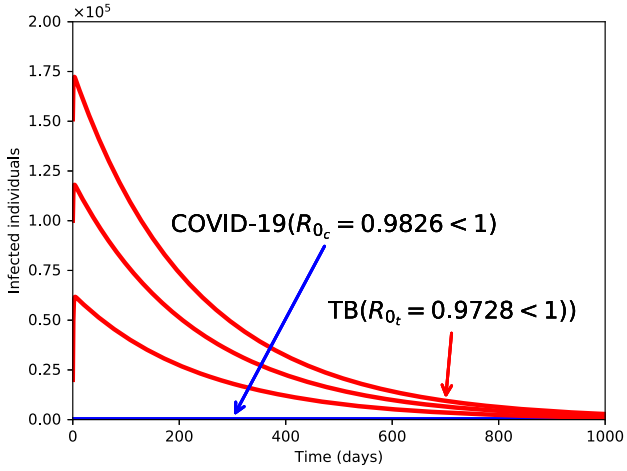

Fig. 13. Simulations of the model (1) illustrating the plots of infectious classes I_c, and I_t at various initial values. Here, all parameter values are as in Table 2 except $\beta_c = 0.376513$ and $\beta_t = 0.638826$ so that $R_{0_c} = 0.9826 < 1$ and $R_{0_t} = 0.9728 < 1$.

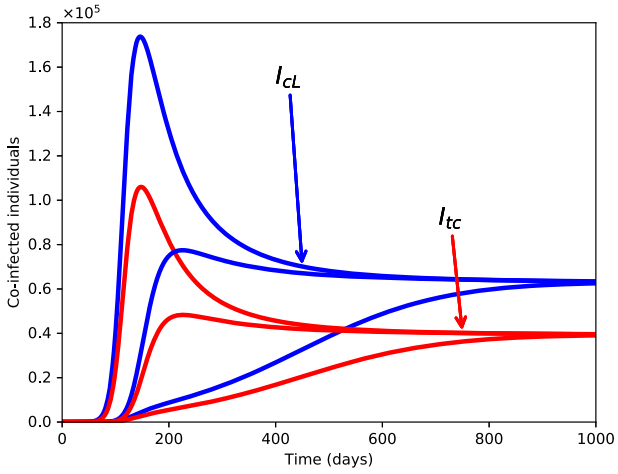

Fig. 14. Simulations of model (1) showing the number of co-infected individuals, I_{cL} and TB, I_{tc} at various initial values. Here, all parameter values are as in Table 2 so that $R_{0_c} = 1.3218 > 1$ and $R_{0_t} = 1.3078 > 1$.

bifurcation analysis, we observed that both the DFE and the EE can not co-exist, and as a result, the sub-models' endemic equilibria are GAS for R_{0_c} and R_{0_t} greater than unity. The co-infection model equilibrium is LAS and GAS based on the fact that both sub-models experience forward bifurcation.

For the numerical simulation, we fitted the curve and also estimated the parameters from the fitted curve. To support the analytical results, we performed different simulation results. It reveals that minimizing the contact with both infections decrease the disease load in the population, and hence the co-infection. Again, the parameter κ has an impact on reducing COVID-19 infection and its co-infection. As evidence for increasing the number of communities employing COVID-19 personal preventive strategy reduces the disease load in the community. Furthermore, the simulation results showed that the invasion of both diseases is always possible inside the community for basic reproductive number greater than one, agreeing with the analytical results. Thus, one can conclude that it is possible to lessen the COVID-19 spread through reducing effective contacts and raising the number of communities employing COVID-19 personal protection strategy, which also mitigates the new co-infection cases. Besides, our study reveals that minimizing the probability of individuals that have TB infection and contracting COVID-19 will also reduce the burden of COVID-19 disease, and the co-infection from the populations.

CRediT authorship contribution statement

Zenebe Shifaraw Kifle; Legesse Lemecha Obsu: Conceived and designed the experiments; Performed the experiments; Analyzed and interpreted the data; Contributed reagents, materials, analysis tools or data; Wrote the paper.

Declaration of competing interest

The authors declare that they have no known competing financial interests or personal relationships that could have appeared to influence the work reported in this paper.

Data availability statement

Data included in article/supplementary material/referenced in article.

Acknowledgements

The authors acknowledge Adama Science and Technology University for its support during this research work, and the Simon's foundation fellowship through Research and Graduate Studies in Mathematics and its Applications (RGSMA), Botswana International University of Science and Technology (BIUST), for their financial support.

References

[1] X. Tang, C. Wu, X. Li, Y. Song, X. Yao, X. Wu, Y. Duan, H. Zhang, Y. Wang, Z. Qian, et al., On the origin and continuing evolution of SARS-CoV-2, Natl. Sci. Rev. 7 (6) (2020) 1012–1023, https://doi.org/10.1186/s40779-020-00240-0.
[2] C. Huang, Y. Wang, X. Li, L. Ren, J. Zhao, Y. Hu, et al., Clinical features of patients infected with 2019 novel coronavirus in Wuhan, China, Lancet 395 (10223) (2020) 497–506.
[3] K. Bjorgul, W.M. Novicoff, K.J. Saleh, Evaluating comorbidities in total hip and knee arthroplasty: available instruments, J. Orthop. Trauma 11 (4) (2010) 203–209.
[4] Centers for Disease Control and Prevention (CDC), Symptoms of coronavirus, Available online: https://www.cdc.gov/coronavirus/2019-ncov/about/symptoms.html.
[5] Global Tuberculosis Report, Available from: https://www.who.int/tb/publications/global_report/en/. (Accessed 14 October 2021).
[6] Y. Chen, Y. Wang, J. Fleming, Y. Yu, Y. Gu, C. Liu, et al., Active or latent tuberculosis increases susceptibility to COVID-19 and disease severity, MedRxiv (2020).
[7] D. Wang, B. Hu, Ch. Hu, F. Zhu, X. Liu, J. Zhang, B. Wang, H. Xiang, Z. Cheng, Y. Xiong, et al., Clinical characteristics of 138 hospitalized patients with 2019 novel coronavirus-infected pneumonia in Wuhan, China, JAMA 323 (11) (2020) 1061–1069.
[8] J. Yang, Y. Zheng, X. Gou, K. Pu, Z. Chen, Q. Guo, Y. Zhou, et al., Prevalence of comorbidities and its effects in patients infected with SARS-CoV-2: a systematic review and meta-analysis, Int. J. Infect. Dis. 94 (2020) 91–95.
[9] World Health Organization (WHO), Information note: tuberculosis and COVID-19, Available from: https://bit.ly/3KeljJp. (Accessed 12 May 2020).
[10] L. Petrone, E. Petruccioli, V. Vanini, G. Cuzzi, G. Gualano, P. Vittozzi, et al., Coinfection of tuberculosis and COVID-19 limits the ability to in vitro respond to SARS-CoV-2, Int. J. Infect. Dis. 113 (2021) S82–S87.
[11] G.T. Mousquer, A. Peres, M. Fiegenbaum, Pathology of TB/COVID-19 co-infection: the phantom menace, Tuberculosis 126 (2021) 102020.
[12] M. Davies, HIV and risk of COVID-19 death: a population cohort study from the Western Cape Province, South Africa, MedRxiv (2020).
[13] I. Motta, R. Centis, L. D'Ambrosio, J.M. Garcia-Garcia, D. Goletti, G. Gualano, et al., Tuberculosis, COVID-19 and migrants: preliminary analysis of deaths occurring in 69 patients from two cohorts, Pulmonology 26 (4) (2020) 233–240.
[14] C. Yang, J. Wang, A mathematical model for the novel coronavirus epidemic in Wuhan, China, Math. Biosci. Eng. 17 (3) (2020) 2708–2724, https://doi.org/10.3934/mbe.2020148.
[15] S.E. Eikenberry, M. Mancuso, E. Iboi, T. Phan, K. Eikenberry, Y. Kuang, E. Kostelich, A.B. Gumel, To mask or not to mask: modeling the potential for face mask use by the general public to curtail the COVID-19 pandemic, Infect. Dis. Model. 5 (2020) 293–308, https://doi.org/10.1016/j.idm.2020.04.001.
[16] S.S. Musa, S. Qureshi, S. Zhao, A. Yusuf, U.T. Mustapha, D. He, Mathematical modeling of COVID-19 epidemic with effect of awareness programs, Infect. Dis. Model. 6 (2021) 448–460, https://doi.org/10.1016/j.idm.2021.01.012.
[17] H. Youssef, N. Alghamdi, M.A. Ezzat, A.A. El-Bary, A.M. Shawky, Study on the SEIQR model and applying the epidemiological rates of COVID-19 epidemic spread in Saudi Arabia, Infect. Dis. Model. 6 (2021) 678–692, https://doi.org/10.1016/j.idm.2021.04.005.
[18] H.M. Youssef, N.A. Alghamdi, M.A. Ezzat, A.A. El-Bary, A.M. Shawky, A new dynamical modeling SEIR with global analysis applied to the real data of spreading COVID-19 in Saudi Arabia, Math. Biosci. Eng. 17 (6) (2020) 7018–7044, https://doi.org/10.3934/mbe.2020362.

[19] A. Omame, N. Sene, I. Nometa, C.I. Nwakanma, E.U. Nwafor, N.O. Iheonu, D. Okuonghae, Analysis of COVID-19 and comorbidity co-infection model with optimal control, Optim. Control Appl. Methods 42 (6) (2020) 1568–1590, https://doi.org/10.1002/oca.2748.
[20] I.M. Hezam, A. Foul, A. Alrasheedi, A dynamic optimal control model for COVID-19 and cholera co-infection in Yemen, Adv. Differ. Equ. 2021 (1) (2021) 1–30, https://doi.org/10.1186/s13662-021-03271-6.
[21] S.Y. Tchoumi, M.L. Diagne, H. Rwezaura, J.M. Tchuenche, Malaria and COVID-19 co-dynamics: a mathematical model and optimal control, Appl. Math. Model. 99 (2021) 294–327, https://doi.org/10.1016/j.apm.2021.06.016.
[22] A. Omame, M. Abbas, C. Onyenegecha, A fractional-order model for COVID-19 and tuberculosis co-infection using Atangana-Baleanu derivative, Chaos Solitons Fractals 153 (2021) 111486, https://doi.org/10.1016/j.chaos.2021.111486.
[23] M. Goudiaby, L. Gning, M. Diagne, B.M. Dia, H. Rwezaura, J. Tchuenche, Optimal control analysis of a COVID-19 and tuberculosis co-dynamics model, Inform. Med. Unlocked 28 (2022) 100849, https://doi.org/10.1016/j.imu.2022.100849.
[24] K.G. Mekonen, S.F. Balcha, L.L. Obsu, A. Hassen, Mathematical modeling and analysis of TB and COVID-19 coinfection, J. Appl. Math. (2022) 1–20, https://doi.org/10.1155/2022/2449710.
[25] H. Rwezaura, M.L. Diagne, A. Omame, A.L. de Espindola, J.M. Tchuenche, Mathematical modeling and optimal control of SARS-CoV-2 and tuberculosis co-infection: a case study of Indonesia, Model. Earth Syst. Environ. (2022) 1–28, https://doi.org/10.1007/s40808-022-01430-6.
[26] F. Inayaturohmat, N. Anggriani, A.K. Supriatna, A mathematical model of tuberculosis and COVID-19 coinfection with the effect of isolation and treatment, Front. Appl. Math. Stat. 8 (2022) 958081, https://doi.org/10.3389/fams.2022.958081.
[27] J. Zhang, Z. Ma, Global dynamics of an SEIR epidemic model with saturating contact rate, Math. Biosci. 185 (2003) 15–32, https://doi.org/10.1016/S0025-5564(03)00087-7.
[28] R. Aggarwal, Dynamics of HIV-TB co-infection with detection as optimal intervention strategy, Int. J. Non-Linear Mech. 120 (2020) 103388.
[29] A. Tanvi, R. Aggarwal, Y.A. Raj, A fractional order HIV-TB co-infection model in the presence of exogenous reinfection and recurrent TB, Nonlinear Dyn. (2021) 1–25.
[30] R. Aggarwal, Stability analysis of a delayed HIV-TB co-infection model in resource limitation settings, Chaos Solitons Fractals 140 (2020) 110138.
[31] L. Perko, Differential Equations and Dynamical Systems, Text in Applied Mathematics, vol. 7, Springer, Berlin, 2000.
[32] A. Korobeinikov, G.C. Wake, Lyapunov functions and global stability for SIR, SIRS, and SIS epidemiological models, Appl. Math. Lett. 15 (2002) 955–960.
[33] V. Hutson, K. Schmitt, Permanence and the dynamics of biological systems, Math. Biosci. 111 (1) (1992) 1–71, https://doi.org/10.1016/0025-5564(92)90078-B.
[34] E. Mtisi, H. Rwezaura, J.M. Tchuenche, A mathematical analysis of malaria and tuberculosis co-dynamics, Discrete Contin. Dyn. Syst., Ser. B 12 (4) (2009) 827–864, https://doi.org/10.3934/dcdsb.2009.12.827.
[35] Z. Mukandavire, A.B. Gumel, W. Garira, J.M. Tchuenche, Mathematical analysis of a model for HIV-malaria co-infection, Math. Biosci. Eng. 6 (2) (2009) 333–362, https://doi.org/10.3934/mbe.2009.6.333.
[36] O. Diekmann, J.A.P. Heesterbeek, M.G. Roberts, The construction of next-generation matrices for compartmental epidemic models, J. R. Soc. Interface 7 (47) (2010) 873–885.
[37] D.P. van den, J. Watmough, Reproduction numbers and sub-threshold endemic equilibria for compartmental models of disease transmission, Math. Biosci. 180 (1) (2002) 29–48.
[38] J. LaSalle, Some extensions of Liapunov's second method, IRE Trans. Circuit Theory 7 (4) (1960) 520–527, https://doi.org/10.1109/tct.1960.1086720.
[39] C. Castillo-Chavez, B. Song, Dynamical models of tuberculosis and their applications, Math. Biosci. Eng. 1 (2) (2004) 361, https://doi.org/10.3934/mbe.2004.1.361.
[40] L.J.S. Allen, An Introduction to Mathematical Biology, Pearson Prentice Hall, Upper Saddle River, New Jersey, 2007.
[41] M. Martcheva, An Introduction to Mathematical Epidemiology, vol. 61, Springer, 2015.
[42] C. Castillo-Chavez, Z. Feng, W. Huang, On the computation of R_0 and its role on global stability, in: Mathematical Approaches for Emerging and Re-Emerging Infection Diseases: An Introduction, vol. 125, 2002, pp. 31–65.
[43] Ethiopian Public Health Institute COVID-19 cases report, 2022.
[44] Python Software Foundation, Python language reference, Available from: https://www.python.org, 2019.
[45] Johns Hopkins University Coronavirus Resource Center, Coronavirus cases-Ethiopia, Available from: https://www.indexmundi.com/coronavirus/country/et.
[46] Z.S. Kifle, L.L. Obsu, Mathematical modeling for COVID-19 transmission dynamics: a case study in Ethiopia, Results Phys. 34 (2022) 105191, https://doi.org/10.1016/j.rinp.2022.105191.
[47] SciPy.org, scipy.optimize.curve_fit, Available from: https://docs.scipy.org/doc/scipy/reference/generated/scipy.optimize.curve_fit.html, 2021.
[48] Z. Abreu, G. Cantin, C.J. Silva, Analysis of a COVID-19 compartmental model: a mathematical and computational approach, Math. Biosci. Eng. 189 (6) (2021) 7979–7998, https://doi.org/10.3934/mbe.2021396.
[49] ETHIOPIA-TREAT TB: technology, research, education, and technical assistant for tuberculosis, https://treattb.org/trial-sites/ethiopia/.